ELSEVIER

International Journal of Heat and Fluid Flow 23 (2002) 52–73

International Journal of HEAT AND FLUID FLOW

www.elsevier.com/locate/ijhff

Fully developed laminar flow of purely viscous non-Newtonian liquids through annuli, including the effects of eccentricity and inner-cylinder rotation

M.P. Escudier [a,*], P.J. Oliveira [b], F.T. Pinho [c]

[a] Department of Engineering, Mechanical Engineering, University of Liverpool, Brownlow Hill, Liverpool L69 3GH, UK
[b] Departamento de Engenharia Electromecânica, Universidade de Beira Interior, Rua Marquês D'Ávila e Bolama, 6201-001 Covilhã, Portugal
[c] Centro de Estudos de Fenómenos de Transporte, DEMEGI, Faculdade de Engenharia, Universidade do Porto, Rua Roberto Frias, 4200-465 Porto, Portugal

Received 19 April 2001; accepted 23 August 2001

Abstract

The results are presented of extensive numerical calculations, carried out using a highly accurate finite-volume method, for the fully developed laminar flow of an inelastic shear-thinning power-law fluid through an eccentric annulus with inner cylinder rotation. Additional calculations are reported for more complex rheological models, including Cross, Carreau and Herschel–Bulkley, which we relate systematically to the power-law model. Comparisons are made with the results of other recent numerical studies. An extensive bibliography is appended of 100 papers additional to those specifically referenced and concerned with theoretical and numerical investigations of laminar flow of non-Newtonian fluids through annular channels.

Keywords: Laminar; Non-Newtonian; Annulus; Eccentric; Rotation

1. Introduction

It has been estimated (Pearson, 1988) that some 10^6 m^3 of drilling muds are used annually to drill 10^4 or more oil and gas wells. During drilling operations these liquid muds are pumped from a surface mud tank through the drillpipe (several kilometres in length), through nozzles in the rotating drillbit, and back to the mud tank through the annular space between the wellbore wall and the drill pipe. Drilling muds have several functions: to support the wellbore wall and prevent its collapse; to prevent ingress of formation fluids (gas and liquid) into the wellbore; to transport rock cuttings to the surface; to minimise settling of the cuttings if circulation is interrupted; to clear the workface; to cool the drillbit; and to lubricate the drill string. These requirements are related directly to both the cost effectiveness of drilling operations and also their safety, for example kick detection and control (blowout prevention). The composition of a drilling mud is formulated to meet these requirements which will differ from well to well. In general, however, such colloidal systems are thixotropic, shear-thinning liquids exhibiting apparent yield stress and some degree of viscoelasticity.

Since the annual cost of the drilling operations outlined above runs into billions of dollars, it comes as no surprise that the oil industry (i.e. the oil companies themselves together with the oilfield-service companies) has invested heavily in research into the flow of drilling mud (''mud hydraulics''). Calculation of the flow down the drillpipe is relatively straightforward whereas the flow through the drillbit nozzles and in the region of the workface is turbulent and extremely complex. From a practical point of view interest focuses on the variation in mud pressure within the wellbore and, to some degree, the hydraulic torque (i.e. the torque exerted on the rotating drillstring by the surrounding mud). The underlying challenge to fluid dynamicists has been to calculate the flowfield within the drillstring-wellbore annulus, a situation usually idealised as that of steady,

* Corresponding author. Tel.: +44-151-794-4804; fax: +44-151-794-4848.
E-mail address: escudier@liv.ac.uk (M.P. Escudier).

0142-727X/02/$ - see front matter
PII: S0142-727X(01)00135-7

Nomenclature

D_H	hydraulic diameter, 2δ (m)
e	displacement of inner-cylinder axis from outer-cylinder axis (m)
f	Fanning friction factor, $-\delta\frac{\partial p}{\partial z}/(\rho U^2)$
K	consistency index (Pa s^n)
n	power-law index
p	pressure (Pa)
$\overline{p}$	non-dimensional pressure, $p\delta/(\mu\omega R_I)$
r	radial distance from axis of inner cylinder (m)
$\overline{r}$	non-dimensional value of r, r/δ
R_I	outer radius of inner cylinder (m)
R_O	inner radius of outer cylinder (m)
Re	bulk axial Reynolds number, $2\rho U\delta/\mu_F$
Re_0	Reynolds number for power-law fluid when $\omega = 0$
T	rotational Reynolds number, $\rho\omega R_I\delta/\mu_F$
Ta	Taylor number, $(\rho\omega/\mu_F)^2 R_I\delta^3$
Ta_0	Taylor number for power-law fluid when $U = 0$
u	axial component of velocity (m/s)
$\overline{u}$	non-dimensional value of u, u/U
U	bulk axial velocity (m/s)
v	tangential component of velocity (m/s)
$\overline{v}$	non-dimensional value of v, $v/(\omega R_I)$
w	radial component of velocity (m/s)
$\overline{w}$	non-dimensional value of w, $w/(\omega R_I)$
y	radial distance from outer wall of inner cylinder (m)
$\overline{y}$	non-dimensional value of y, y/δ
z	axial distance (m)
$\overline{\gamma}$	non-dimensional shear rate, $\dot{\gamma}/\dot{\gamma}_F$
γ_F	non-dimensional value of $\dot{\gamma}_F$, $\dot{\gamma}_F\delta/U$
$\dot{\gamma}$	shear rate (s^{-1})
$\dot{\gamma}_C$	characteristic shear rate for fluid (s^{-1})
$\dot{\gamma}_F$	characteristic shear rate for flow (s^{-1})
δ	mean annular gap width, $R_O - R_I$ (m)
Δ	percentage difference between f_{HB}, f_{CR}, etc., and f_{PL}
ε	eccentricity, e/δ
κ	radius ratio, R_I/R_O
λ	time constant (s)
μ	dynamic viscosity (Pa s)
$\overline{\mu}$	non-dimensional viscosity, μ/μ_F
μ_F	characteristic viscosity for flow (Pa s)
μ_0	viscosity for zero shear rate (Pa s)
μ_∞	viscosity for infinite shear rate (Pa s)
ξ	velocity ratio, $\omega R_I/U$
ρ	fluid density (kg/m^3)
τ	shear stress (Pa)
τ_S	wall shear stress averaged over wetted surface of annulus (Pa)
τ_Y	yield stress (Pa)
ϕ	angular location with respect to inner cylinder
ψ	stream function, $\int_r^{R_O} v\,dr$
$\overline{\psi}$	non-dimensional stream function, $\psi/\int_{R_I}^{R_O} v\,dr$
ω	angular velocity of inner cylinder (rad/s)

Subscripts

CA	Carreau model
CR	Cross model
F	flow
HB	Herschel–Bulkley model
I	inflexion point on $\log\mu$ versus $\log\dot{\gamma}$ curve
NN	non-Newtonian
PL	power-law model
SCA	simplified Carreau model
SCR	simplified Cross model

isothermal, fully developed laminar flow of a shear-thinning liquid (modelled as a generalised Newtonian fluid) through an annulus consisting of an outer cylindrical cylinder and an inner cylinder which may be offset (i.e. eccentric) and rotating. In conventional drilling the radius ratio of the annulus geometry is typically about 0.5 whereas in slimhole drilling and coiled-tube operations it exceeds 0.8. In reality the problem is complicated by numerous factors: for example, the wellbore wall will depart significantly from circularity, the eccentricity varies with depth, the pressure and temperature increase significantly with depth, drilling muds are to some degree (depending upon the chemical composition) viscoelastic and thixotropic and invariably contaminated with drill cuttings and formation fluid (gas and liquid). A complete analysis of the idealised problem is a prerequisite to a quantitative understanding of these more complex situations.

Although the drilling of oil wells is the most important, there are numerous other applications which require a detailed understanding of the annular flow of non-Newtonian liquids. Such applications include oil well-completion operations and are also found in industries dealing with industrial waste, with slurries and suspensions such as processed foodstuffs, synthetic fibres and even blood, and with the extrusion of molten plastics and polymer solutions.

Even the idealised problem specified above is far from trivial and it is only very recently that it has been possible to carry out calculations to predict all aspects of the flowfield including the velocity distribution, frictional pressure drop and torque exerted on the rotating inner cylinder. The present status has been reached gradually: within the references together with the bibliography appended to this paper are 126 papers dealing with progressively more complex aspects of the problem,

initially using analytical techniques (both exact and approximate), followed by numerical solutions to physical approximations, and more recently, as here, purely numerical procedures to solve the complete idealised problem.

A cursory overview of all the work to date is provided by the references plus the bibliography in which we list all the published papers of which we are aware concerned with theoretical and computational aspects of the flow of generalised Newtonian fluids through annular ducts. By far the most entries (70 papers) are for the concentric annulus with bulk flow and no rotation of either cylindrical surface. However, since rotation of the drillpipe is inherent to the wellbore drilling application, it is not surprising that numerous papers (22) are concerned with the concentric annulus with bulk flow and centrebody rotation (often referred to as helical or spiral flow). Since a complication in the design of drilling operations is that the drillpipe is invariably offset (i.e. eccentric) to an unknown degree, another large group (25) of papers is concerned with bulk flow through an eccentric annulus with no rotation of either surface. Only recently has the most general situation of bulk flow through an eccentric annulus with inner cylinder rotation received attention (10 papers) though the range of parameters covered is very limited, hitherto there has been no systematic investigation of the effects of these parameters and their interactions and some of the conclusions are at best misleading, as we discuss in the present paper. We have not included in the bibliography the hundreds of papers concerned with the flow induced in a concentric annulus in the absence of bulk flow and the associated problem of Taylor instability. Nor have we included papers primarily concerned with viscoelastic fluids or papers concerned with flow in an eccentric annulus in the absence of bulk flow.

The first paper to be published on the topic of non-Newtonian liquid flow through an annulus is that of Volarovich and Gutkin (1946) who gave an approximate analytical solution for the axial flow of a Bingham fluid in a concentric annulus. The first exact solution to this problem was given by Laird (1957) whilst Fredrickson and Bird (1958) considered both Bingham and power-law fluids. Other generalised Newtonian fluids to be investigated include Ellis (Bird, 1965), Meter and Bird (Rotem, 1962; Kozicki et al., 1966), Rabinowitsch (Rotem, 1962; Kozicki et al., 1966), Eyring (Nebrenský and Ulbrecht, 1968), Casson (Shul'man, 1970), Ree–Eyring (Nebrenský et al., 1970), Powell–Eyring (Russell and Christiansen, 1974), Herschel–Bulkley (Hanks, 1979) and Robertson–Stiff (Fordham et al., 1991). Starting with Rivlin (1956), many of these fluid models have also been adopted for the investigation of flow through a concentric annulus with rotation of the centrebody. Rigbi and Galili (1971) added the Cross model to the list and quite recently Batra and Eissa (1994) the Sutterby fluid. For flow through an eccentric annulus, with no rotation of the inner cylinder, Vaughn (1965) gave an approximate solution for a power-law fluid, Mitsuishi and Aoyagi (1973) considered the Sutterby fluid, Guckes (1975) the Bingham fluid, Haciislamoglu and Langlinais (1990) the Herschel–Bulkley fluid, and Pham and Mitsoulis (1998) the Papanastasiou fluid. Although many researchers evaluated numerically the integrals which resulted from their analyses, it is only in the last 10 years or so that either finite-difference, finite volume or finite-element methods have been used to provide exact numerical solutions to the equations of motion and such methods now permit consideration of the complex problem of flow through an eccentric annulus with inner cylinder rotation of any generalised Newtonian fluid. For this problem, Locket (1992) investigated both power-law and Bingham fluids, Hussain and Sharif (1998) and Wan et al. (2000) power law, and Meuric et al. (1998) both power law and Herschel–Bulkley. Hussain and Sharif (2000) have recently extended their Herschel–Bulkley calculations to a partially blocked eccentric annulus. For problems involving viscoplastic fluids, numerical strategies are required to avoid the appearance of infinite viscosities for shear stresses below the yield stress (when the shear rate is zero). Beverly and Tanner (1992) for example, adopted the biviscosity model to calculate the flow of a Bingham fluid through an eccentric annulus with inner cylinder rotation (unfortunately the numerical results in Beverly and Tanner's paper show slip at the surface of the inner cylinder and unclosed isovels suggesting that an incorrect boundary condition was applied). Much of the previous work is reviewed briefly in the recent book by Chin (2001) which also discusses applications to drilling and production, and flow assurance procedures in subsea pipeline design.

In a recent paper (Escudier et al., 2000) we showed that the flow of a Newtonian fluid through an annulus exhibits completely unexpected behaviour for high rotation rates of the inner cylinder at very high eccentricities. In particular, the axial velocity distribution develops a second peak and the friction factor increases rather than decreases. As outlined above, the principal application of research into non-Newtonian liquid flow through annuli is to wellbore drilling operations, where the location of the drill pipe (i.e. inner cylinder) is uncontrolled (and largely unknown). It is important therefore to know the consequences of high eccentricity and this is an aspect we address in the present paper. The basic computer code implemented here is the same as that used for the Newtonian case except that the viscosity is now a specified function of the local shear rate. We present extensive results for a power-law fluid and more limited results for three other viscosity models (Herschel–Bulkley, Carreau and Cross) which we relate systematically to the power-law model and compare the

results of both sets of calculations. Escudier et al. (2000) showed that there was excellent agreement between their calculations for a Newtonian fluid and experimental data for annuli with 20%, 50% and 80% eccentricity. In a separate paper (Escudier et al., 2001) we present extensive comparisons of the results of calculations for shear-thinning liquids, such as those under discussion here, with experimental data for the flow of a wide variety of non-Newtonian liquids through annular geometries with eccentricities of 0, 50% and 80%. In general, the comparisons are extremely good and confirm that viscoelastic effects, neglected in the calculations, play no significant role in the flows under consideration. There are, however, discrepancies in some cases but these appear to be attributable to the experimental data rather than the calculations.

The governing equations for the flows under consideration are stated in Section 2, first in dimensional form and then in a non-dimensional form. An outline of the numerical procedure is also included together with remarks on the solution accuracy. In Section 3 we present the results of an extensive series of calculations for power-law fluids and in Section 4 we quantify how these results are influenced by considering other rheological models (Herschel–Bulkley, Carreau and Cross). A general methodology by which the power-law results can be applied to flows for fluids obeying other viscosity models is developed in Appendix A. In Section 5 we compare our results for a power-law fluid with those of Meuric et al. (1998).

2. Governing equations and numerical procedure

We consider isothermal, laminar, fully developed flows of fluids for which the density is constant and the viscosity dependent only on the second invariant of the strain-rate tensor (i.e. generalised Newtonian fluids). If the axial, tangential and radial components of velocity are u, v and w, respectively, r is the radial distance from the centre of the inner cylinder, ϕ the angular location with respect to the inner cylinder (as shown in Fig. 1, $\phi = 0$ corresponds to the widest part of the annulus), and z is the axial location, then the governing equations for such flows can be written as follows:

Continuity

$$\frac{\partial}{\partial r}(wr) + \frac{\partial v}{\partial \phi} = 0. \tag{1}$$

u-Momentum

$$\rho\left(w\frac{\partial u}{\partial r} + \frac{v}{r}\frac{\partial u}{\partial \phi}\right) = -\frac{\partial p}{\partial z} + \frac{1}{r}\frac{\partial}{\partial r}\left(\mu r\frac{\partial u}{\partial r}\right) + \frac{1}{r^2}\frac{\partial}{\partial \phi}\left(\mu\frac{\partial u}{\partial \phi}\right). \tag{2}$$

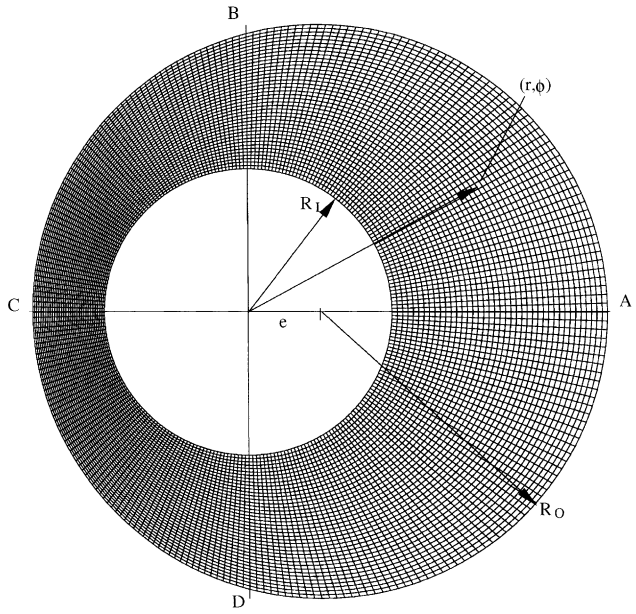

Fig. 1. Annulus geometry and computational grid (40 × 256 cells).

v-Momentum

$$\rho\left(w\frac{\partial v}{\partial r} + \frac{v}{r}\frac{\partial v}{\partial \phi} + \frac{wv}{r}\right) = -\frac{1}{r}\frac{\partial p}{\partial \phi} + \frac{1}{r^2}\frac{\partial}{\partial r}\left[\mu r^3\frac{\partial}{\partial r}\left(\frac{v}{r}\right) + \mu r\frac{\partial w}{\partial \phi}\right] + \frac{2}{r}\frac{\partial}{\partial \phi}\left(\frac{\mu}{r}\frac{\partial v}{\partial \phi} + \frac{\mu w}{r}\right). \tag{3}$$

w-Momentum

$$\rho\left(w\frac{\partial w}{\partial r} + \frac{v}{r}\frac{\partial w}{\partial \phi} - \frac{v^2}{r}\right) = -\frac{\partial p}{\partial r} + \frac{2}{r}\frac{\partial}{\partial r}\left(\mu r\frac{\partial w}{\partial r}\right) + \frac{\partial}{\partial \phi}\left[\mu\frac{\partial}{\partial r}\left(\frac{v}{r}\right)\right] + \frac{1}{r^2}\frac{\partial}{\partial \phi}\left(\mu\frac{\partial w}{\partial \phi}\right) \tag{4}$$

with boundary conditions

$u = v = w = 0$ on the outer cylinder; $u = w = 0$ and $v = \omega R_I$ on the inner cylinder;

and the magnitude of the rate-of-strain tensor (or shear rate) $\dot{\gamma}$ is given by

$$\dot{\gamma}^2 = \left[r\frac{\partial}{\partial r}\left(\frac{v}{r}\right) + \frac{1}{r}\frac{\partial w}{\partial \phi}\right]^2 + \frac{1}{r^2}\left(\frac{\partial u}{\partial \phi}\right)^2 + \left(\frac{\partial u}{\partial r}\right)^2 + 4\left(\frac{\partial w}{\partial r}\right)^2. \tag{5}$$

It is clear from Eqs. (2)–(4) that spatial derivatives of the viscosity μ must be accounted for and that variations with the angular location ϕ arise as a consequence of the eccentricity of the annulus ε (i.e. the flow is two-dimensional).

We now introduce the same non-dimensional parameters as for the flow of a Newtonian fluid (Escudier et al., 2000) but with a viscosity μ_F evaluated at a characteristic shear rate for the flow $\dot{\gamma}_F$ defined by

$$\dot{\gamma}_F^2 = \left(\frac{U}{D_H}\right)^2 + \left(\frac{\omega R_I}{D_H}\right)^2 = \frac{1}{4}\left[\left(\frac{U}{\delta}\right)^2 + \left(\frac{\omega R_I}{\delta}\right)^2\right]. \quad (6)$$

This choice for $\dot{\gamma}_F$ is consistent with the work of Locket (1992) whereas Meuric et al. (1998) adopted different scaling for flows with and without centrebody rotation. The non-dimensional flow parameters are

Fanning friction factor

$$f \equiv -\frac{\delta}{\rho U^2}\frac{\partial p}{\partial z} = \frac{2\tau_S}{\rho U^2}. \quad (7)$$

Axial Reynolds number

$$Re \equiv \frac{2\rho U\delta}{\mu_F}. \quad (8)$$

Rotational Reynolds number

$$T \equiv \frac{\rho\omega R_I\delta}{\mu_F}. \quad (9)$$

For consistency with the Newtonian situation, we shall present the results of our numerical calculations in terms of the product $f \cdot Re$ and a Taylor number Ta where

$$Ta \equiv \left(\frac{\rho\omega}{\mu_F}\right)^2 R_I\delta^3 = \left(\frac{1}{\kappa} - 1\right)T^2 \quad (10)$$

and κ is the radius ratio R_I/R_O. The choice for $\dot{\gamma}_F$ adopted here has the advantage that the corresponding values of Re, T and Ta reflect to some extent the non-Newtonian coupling between the axial and tangential velocity distributions. The definitions of Re and Ta correspond with generalised Reynolds and Taylor numbers which can be evaluated for any given fluid, for example for a power-law fluid with

$$\mu = K_{PL}\dot{\gamma}^{n_{PL}-1} \quad (11)$$

we have

$$\omega = 0: \quad Re_0 = \frac{\rho U^{2-n_{PL}} D_H^{n_{PL}}}{K_{PL}}, \quad (12)$$

$$U = 0: \quad Ta_0 = \frac{1}{8}\left(\rho\frac{\omega^{2-n_{PL}}}{K_{PL}}\right)^2 D_H^{2n_{PL}+1} R_I^{3-2n_{PL}} \quad (13)$$

and in the general case of arbitrary rotation and throughflow

$$Re = (1+\xi^2)^{(1-n_{PL})/2} Re_0, \quad (14)$$

$$Ta = \left(\frac{1}{\xi^2} + 1\right)^{1-n_{PL}} Ta_0, \quad (15)$$

where the velocity ratio

$$\xi \equiv \frac{\omega R_I}{U} = \frac{2T}{Re}. \quad (16)$$

It can be seen that ξ is a direct measure of the non-dimensional characteristic shear rate for the flow γ_F, defined by

$$\gamma_F = \frac{\dot{\gamma}_F\delta}{U} = \frac{1}{2}\sqrt{(1+\xi^2)}. \quad (17)$$

In non-dimensional form the governing equations may now be written as

$$\frac{\partial}{\partial\bar{r}}(\bar{w}\bar{r}) + \frac{\partial\bar{v}}{\partial\phi} = 0, \quad (18)$$

$$T\left(\bar{w}\frac{\partial\bar{u}}{\partial\bar{r}} + \frac{\bar{v}}{\bar{r}}\frac{\partial\bar{u}}{\partial\phi}\right) = \frac{1}{2}f\cdot Re + \bar{\mu}\left[\frac{1}{\bar{r}}\frac{2}{\partial\bar{r}}\left(\bar{r}\frac{\partial\bar{u}}{\partial\bar{r}}\right) + \frac{1}{\bar{r}^2}\frac{\partial^2\bar{u}}{\partial\phi^2}\right] + \left[\frac{\partial\bar{u}}{\partial\bar{r}}\frac{\partial\bar{\gamma}}{\partial\bar{r}} + \frac{1}{\bar{r}^2}\frac{\partial\bar{u}}{\partial\phi}\frac{\partial\bar{\gamma}}{\partial\phi}\right]\frac{d\bar{\mu}}{d\bar{\gamma}}, \quad (19)$$

$$T\left(\bar{w}\frac{\partial\bar{v}}{\partial\bar{r}} + \frac{\bar{v}}{\bar{r}}\frac{\partial\bar{v}}{\partial\phi} + \frac{\bar{w}\bar{v}}{\bar{r}}\right) = -\frac{1}{\bar{r}}\frac{\partial\bar{p}}{\partial\phi} + \bar{\mu}\left[\frac{\partial}{\partial\bar{r}}\left\{\frac{1}{\bar{r}}\frac{\partial}{\partial\bar{r}}(\bar{r}\bar{v})\right\} + \frac{1}{\bar{r}^2}\frac{\partial^2\bar{v}}{\partial\phi^2} + \frac{2}{\bar{r}^2}\frac{\partial\bar{w}}{\partial\phi}\right] + \left[\left\{\bar{r}\frac{\partial}{\partial\bar{r}}\left(\frac{\bar{v}}{\bar{r}}\right) + \frac{1}{\bar{r}}\frac{\partial\bar{w}}{\partial\phi}\right\}\frac{\partial\bar{\gamma}}{\partial\bar{r}} - \frac{2}{\bar{r}}\frac{\partial\bar{w}}{\partial\bar{r}}\frac{\partial\bar{\gamma}}{\partial\phi}\right]\frac{d\bar{\mu}}{d\bar{\gamma}}, \quad (20)$$

$$T\left(\bar{w}\frac{\partial\bar{w}}{\partial\bar{r}} + \frac{\bar{v}}{\bar{r}}\frac{\partial\bar{w}}{\partial\phi} - \frac{\bar{v}^2}{\bar{r}}\right) = -\frac{\partial\bar{p}}{\partial\bar{r}} + \bar{\mu}\left[\frac{\partial}{\partial\bar{r}}\left\{\frac{1}{\bar{r}}\frac{\partial}{\partial\bar{r}}(\bar{r}\bar{w})\right\} - \frac{2}{\bar{r}^2}\frac{\partial\bar{v}}{\partial\phi} + \frac{1}{\bar{r}^2}\frac{\partial^2\bar{w}}{\partial\phi^2}\right] + \left[2\frac{\partial\bar{w}}{\partial\bar{r}}\frac{\partial\bar{\gamma}}{\partial\bar{r}} + \left\{\frac{\partial}{\partial\bar{r}}\left(\frac{\bar{v}}{\bar{r}}\right) + \frac{1}{\bar{r}^2}\frac{\partial\bar{w}}{\partial\phi}\right\}\frac{\partial\bar{\gamma}}{\partial\phi}\right]\frac{d\bar{\mu}}{d\bar{\gamma}} \quad (21)$$

with

$$\bar{\gamma}^2 = \frac{4}{1+\xi^2}\left[\frac{1}{\bar{r}^2}\left(\frac{\partial\bar{u}}{\partial\phi}\right)^2 + \left(\frac{\partial\bar{u}}{\partial\bar{r}}\right)^2\right] + \frac{4\xi^2}{1+\xi^2}\left[\left\{\bar{r}\frac{\partial}{\partial\bar{r}}\left(\frac{\bar{v}}{\bar{r}}\right) + \frac{1}{\bar{r}}\frac{\partial\bar{w}}{\partial\phi}\right\}^2 + 4\left(\frac{\partial\bar{w}}{\partial\bar{r}}\right)^2\right]. \quad (22)$$

The non-dimensional variables are defined as

$$\bar{u} \equiv \frac{u}{U}, \quad \bar{v} \equiv \frac{v}{\omega R_I}, \quad \bar{w} \equiv \frac{w}{\omega R_I}, \quad \bar{r} \equiv \frac{r}{\delta}, \quad \bar{p} \equiv \frac{p\delta}{\mu\omega R_I}, \quad \bar{\gamma} \equiv \frac{\dot{\gamma}}{\dot{\gamma}_F}, \quad \bar{\mu} \equiv \frac{\mu}{\mu_F} \quad (23)$$

and the boundary conditions are

$\bar{u} = \bar{w} = 0$ and $\bar{v} = 1$ on the inner cylinder; $\bar{u} = \bar{v} = \bar{w} = 0$ on the outer cylinder.

For a Newtonian fluid, $\overline{\mu} = 1$ and the equations become identical with those of Escudier et al. (2000). We also note that if $\xi \gg 1$ or $\xi \to 0$, then

$$f \cdot Re = F(\varepsilon, \kappa, n_{PL}, Ta) \tag{24}$$

so that $f \cdot Re$ becomes independent of Re, a result which is also true generally for a Newtonian fluid (i.e. $n_{PL} = 1$).

To calculate the velocity components, the governing equations were transformed into a general, non-orthogonal coordinate system. These transformed equations were then discretised following the finite-volume approach of Patankar (1980), but adapted for collocated, non-orthogonal grids, as described in Oliveira (1992). The calculations were carried out using a second-order central differencing scheme and the deferred correction approach was used in order to ensure numerical stability for the convective terms. The solution algorithm was a modified version of the SIMPLEC algorithm of van Doormal and Raithby (1984) adapted for time marching as explained in Issa and Oliveira (1994) where details can be found of the particular procedure used to evaluate mass fluxes at cell faces. When performing calculations with the Herschel–Bulkley model (i.e. for a fluid with a yield stress) the bi-viscosity model was used to avoid stiffness in the matrices at low shear rates and numerical singularities in non-yielded regions following the criteria suggested by O'Donovan and Tanner (1984).

The coordinate system was centered at the inner cylinder axis and the three-dimensional annular geometry represented by 16 structured blocks around the annulus. A cross section of the annular geometry and the grid arrangement for a typical numerical calculation are shown in Fig. 1. Since the fully developed flow condition was of concern here, only one row of cells ($\approx D_H$ in length) was needed in the axial direction and the procedure of Patankar and Spalding (1972) was adopted to correct the axial pressure gradient $\partial p/\partial z$. In the other two directions the grid used in the calculations had 40×256 cells (grid 3) uniformly distributed in the radial and tangential directions. This grid was selected after a systematic grid refinement study was performed to assess the accuracy of the calculation using four progressively finer grids: 10×64 (grid 1), 20×128 (grid 2), 40×256 (as shown in Fig. 1) and 80×512 (grid 4) cells with Newtonian fluids (Escudier et al., 2000) and here extended to power-law fluids.

Numerical accuracy was estimated on the basis of Newtonian and non-Newtonian (power-law) calculations for concentric and eccentric flow cases and comparison with the available analytical solutions and, in its absence, with values determined from using Richardson's extrapolation to the limit technique applied to the results of simulations with the four meshes mentioned above. This is a standard procedure in CFD as mentioned by Roache (1997). For more details of the method, the reader is referred to Ferziger (1981). In the present case, values of the friction factor f were calculated for each of the grids and then Richardson's extrapolation applied to obtain a final value of even higher accuracy than that for grid 4 which we take as the correct value. For the flow of a Newtonian fluid through a concentric annulus the simulations with grid 3 predicted $f \cdot Re$ within 0.1% of the analytical solution. For power-law fluids having a power-law index n_{PL} of 0.5 calculations were performed for a concentric and a 95% eccentric annulus at $Re = 100$ and $Ta = 10\,000$. In this case the grid 3 calculations were found to be within about 0.1% of the values given by Richardson's extrapolation. These comparisons verify the numerical accuracy of the calculations presented in this paper. Validation against experimental results is discussed in detail by Escudier et al. (2001).

3. Numerical solutions for a power-law fluid

The numerical solutions for power-law fluids are presented in Figs. 2–5 and tabulated in Table 1.

Fig. 2 shows the influence of decreasing the power-law parameter n_{PL} i.e. increasing the degree of shear thinning. For a Newtonian fluid (i.e. $n_{PL} = 1$), Escudier et al. (2000) found that $f \cdot Re$ increased with Ta, particularly at the higher eccentricities, due to the increasing distortion of the axial velocity distribution. Their results showed a maximum in $f \cdot Re$ for high Taylor numbers at an eccentricity of about 0.4 (also evident in Fig. 2(c)). Similar tendencies are seen here although the peak in $f \cdot Re$ clearly tends to disappear with increased levels of shear thinning as does the increase at high eccentricities ($\varepsilon > 0.9$). With decreasing n_{PL} the tendency is for the friction factor to decrease and become increasingly independent of ε. As Figs. 2(a)–(c) also show, the dependence on n_{PL} decreases with increasing rotation speed (i.e. increasing Ta). Streamlines constructed from the radial/tangential velocity components show that the underlying reason for the characteristics in Fig. 2 is the disappearance of flow recirculation in the outer region of the annulus, due to decreased viscosity and shear stress in the vicinity of the inner cylinder, and a flattening of the axial velocity distribution. This effect is so intense that even at very high rotation rates ($Ta = 50\,000$) there is no secondary flow for a fluid with $n_{PL} = 0.2$. In general terms the flow of strongly shear-thinning liquids bears strong similarities to that of less pseudoplastic fluids ($n_{PL} \to 1$) at lower Taylor numbers. For a Newtonian fluid the secondary flow (i.e. in the cross-flow plane) is decoupled from the axial flow. For non-Newtonian fluids, however, the axial and secondary

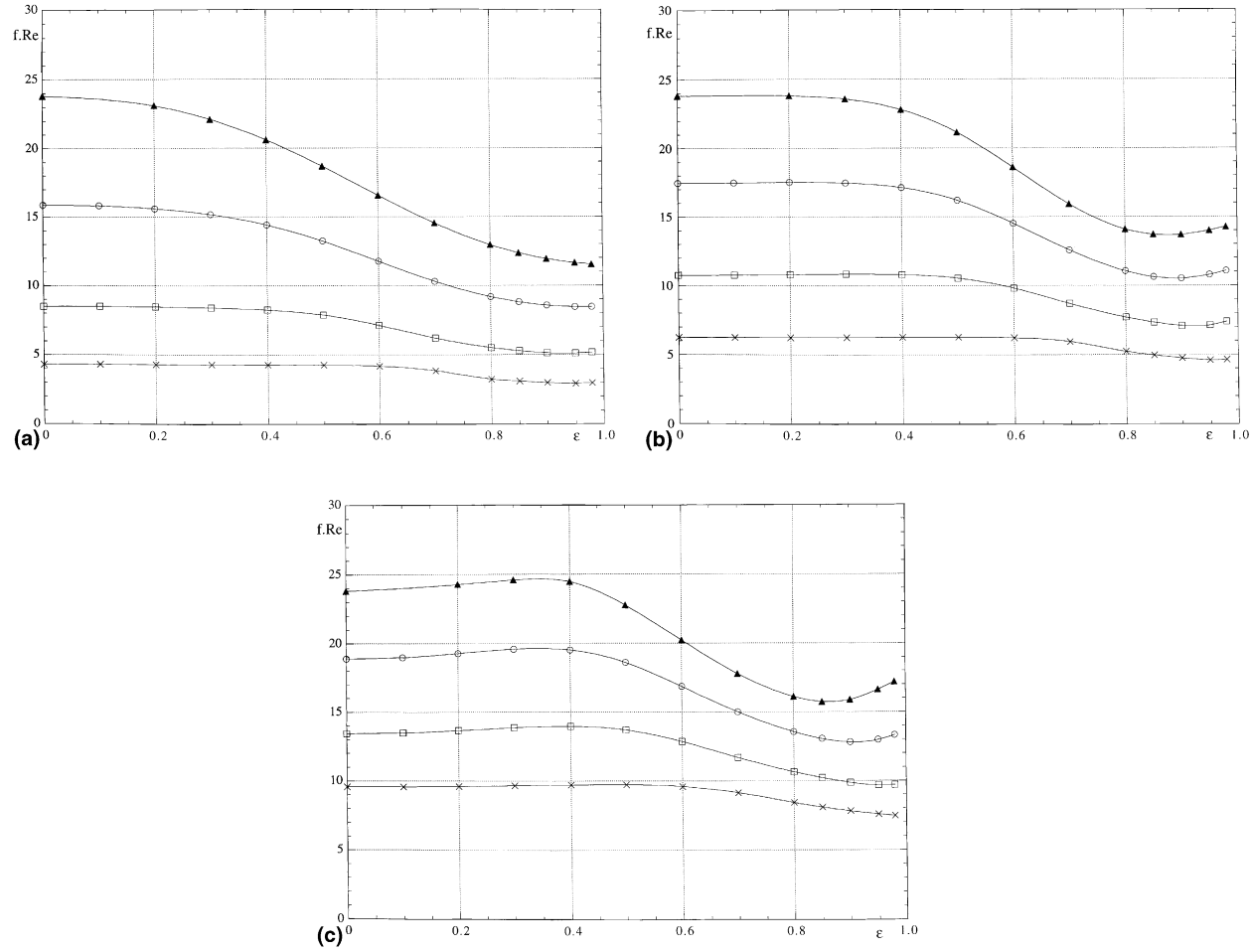

Fig. 2. Influence of shear-thinning rheology on $f \cdot Re$ versus ε for $\kappa = 0.5$, $Re = 100$ and (a) $Ta = 1000$, (b) $Ta = 10\,000$, (c) $Ta = 50\,000$: (▲) $n_{PL} = 1$, (○) $n_{PL} = 0.8$, (□) $n_{PL} = 0.5$, (×) $n_{PL} = 0.2$.

flows are completely coupled. The velocity ratio $\xi \equiv \omega R_I/U$ is a convenient parameter with which to separate the resulting flows into three types:

(1) $\xi < 1$ (axial dominated),
(2) $\xi > 10$ (rotation dominated),
(3) $1 < \xi < 10$ (mixed).

As shown in Section 2, ξ is directly related to the non-dimensional shear rate γ_F according to

$$\gamma_F = \frac{1}{2}\sqrt{(1+\xi^2)} \tag{17}$$

and ξ can also be shown to be given by

$$\xi^2 = \frac{4\kappa Ta}{(1-\kappa)Re^2}. \tag{25}$$

Streamlines of the secondary flow and viscosity contours for three cases representing each of the flow types are shown in Fig. 3.

For flow type (1) shear thinning is due primarily to the axial velocity gradients and so occurs predominantly in the high-shear regions in the vicinity of the surfaces of the inner and outer cylinders, much like a lubricating layer. As pointed out by Fang et al. (1999) (for $\xi = 0$), the decreased viscosity in this layer reduces $f \cdot Re$ compared with the Newtonian case for all eccentricities.

For flow type (2) (i.e. $\xi > 10$) shear thinning is controlled by the velocity gradients in the tangential secondary flow. The situation is more complicated than for type (1) and depends on whether recirculation occurs. For high Ta values and $\varepsilon > 0.5$, a recirculation zone appears within which tangential velocities are very low compared with those in the layer dragged around by the inner cylinder ($\sim\omega \cdot R_I$). Thus shear thinning occurs primarily near the inner cylinder whereas the viscosity remains at very high levels within the recirculation. In consequence $f \cdot Re$ not only increases substantially, but can even exceed the values for a Newtonian fluid. For very high values of either ε or Ta, the recirculating velocities rise, shear thinning occurs within the recirculation region and $f \cdot Re$ falls.

The behaviour for flow type (3) ($1 < \xi < 10$) is mixed with $f \cdot Re$ typically increasing with ξ such that the $f \cdot Re$ versus ε curves are effectively shifted upwards.

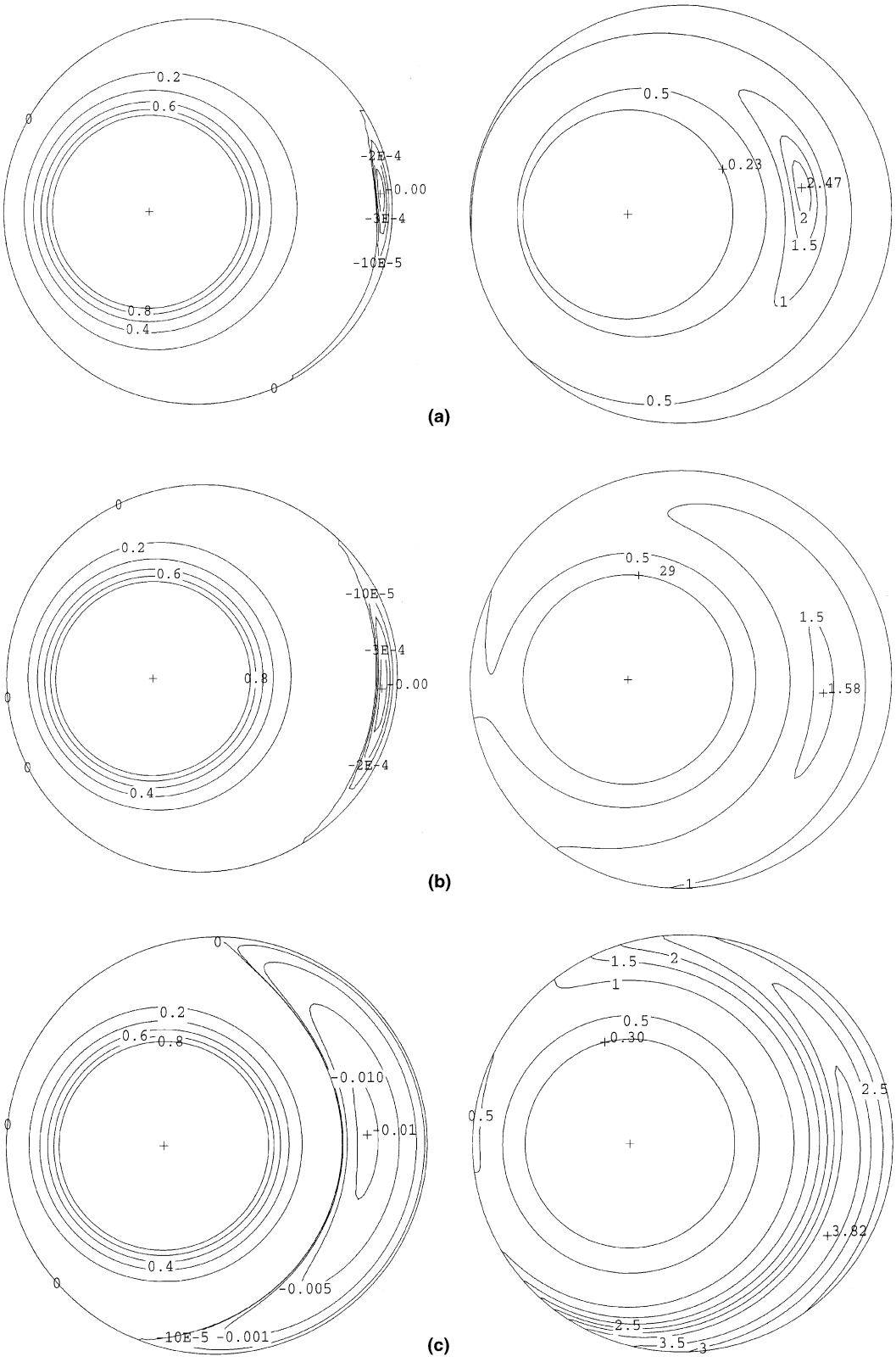

Fig. 3. Secondary-flow streamlines $\overline{\psi}$ (left) and viscosity $\overline{\mu}$ (right) contours for $\kappa = 0.5$, $\varepsilon = 0.5$, $n_{\mathrm{PL}} = 0.5$, $Re = 10$, (a) $Ta = 10$, $\xi = 0.63$, (b) $Ta = 10^3$, $\xi = 6.3$ and (c) $Ta = 5 \times 10^4$, $\xi = 44.7$.

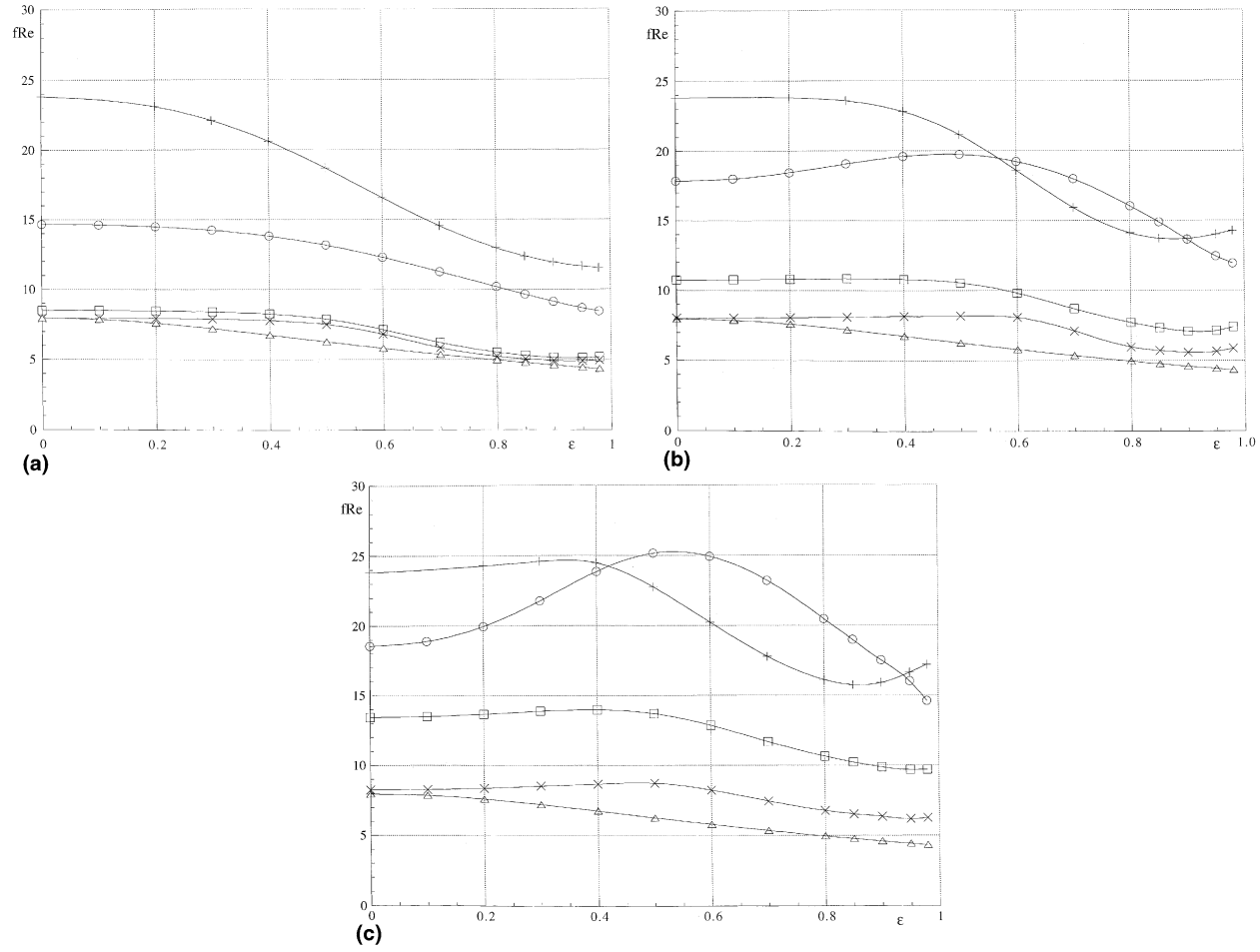

Fig. 4. Influence of Reynolds number on $f \cdot Re$ versus ε for $\kappa = 0.5$, $n_{PL} = 0.5$ and (a) $Ta = 1000$, (b) $Ta = 10\,000$, (c) $Ta = 50\,000$: (○) $Re = 10$, (□) $Re = 100$, (×) $Re = 1000$. Reference curves for $n_{PL} = 1$ (△) and $Ta = 0$ (+).

Figs. 4 and 5 are for fixed values of n_{PL} (0.5) and κ (also 0.5) and show the separate effects of *Re* and *Ta*, respectively. It will be recalled that for a Newtonian fluid $f \cdot Re$ is independent of *Re* because the radial/tangential velocities are de-coupled from the axial velocities. This is not the case for a shear-thinning fluid, except under limiting conditions ($\xi \to 0$ and $\xi \gg 1$), and the influence of *Re* is clearly both significant and complex. Calculations for $\varepsilon = 0.5$ show that a recirculation zone develops in the outer region of the widest part of the annulus, increasing in extent and strength with increasing *Ta* but decreasing with *Re*. The peak axial velocity moves towards the narrowing gap and decreases in magnitude with increasing *Ta*, as seen for Newtonian fluids, but now there is also an influence of Reynolds number. The peak axial velocity always decreases with increasing *Re* but its location depends on both *Ta* and *Re*. At low values of *Ta* the peak moves towards the narrowing gap as *Re* increases but at high *Ta* the angular location of the peak velocity gradually moves back into the wide gap and radially towards the outer wall of the annulus. Although the effects of *Ta* and *Re* on the cross-plane secondary flow appear to be fairly simple in terms of its magnitude, this is not so with regard to the location of the separated flow region. At low *Re* the secondary-flow region is nearly symmetric but at high *Re* the zone of separation moves in the opposite direction to that of the inner cylinder i.e. towards the widening gap in contrast to the Taylor number effect for Newtonian fluids. The viscosity contours show that at low *Re* there is a single region of high viscosity within which the peak value decreases with *Ta* when *Ta* is small but then increases with *Ta* after the onset of secondary flow. For intermediate values of *Ta* and *Re* there are two viscosity peaks at opposite sides of the annulus whereas at very high *Ta* and *Re* values the viscosity field is strongly distorted but with only a single peak. As can be seen from the governing equations in non-dimensional form, the non-dimensional shear rate $\overline{\gamma}$, and hence the viscosity $\overline{\mu}$, now depends on the velocity ratio ξ. In consequence $f \cdot Re$ can be seen to be independent of *Re* for the case of zero rotation and this explains the tendency in Fig. 5 for the $f \cdot Re$ curves to asymptote towards the curve for $Ta = 0$ as *Re* increases. It is also the case that $f \cdot Re$ is

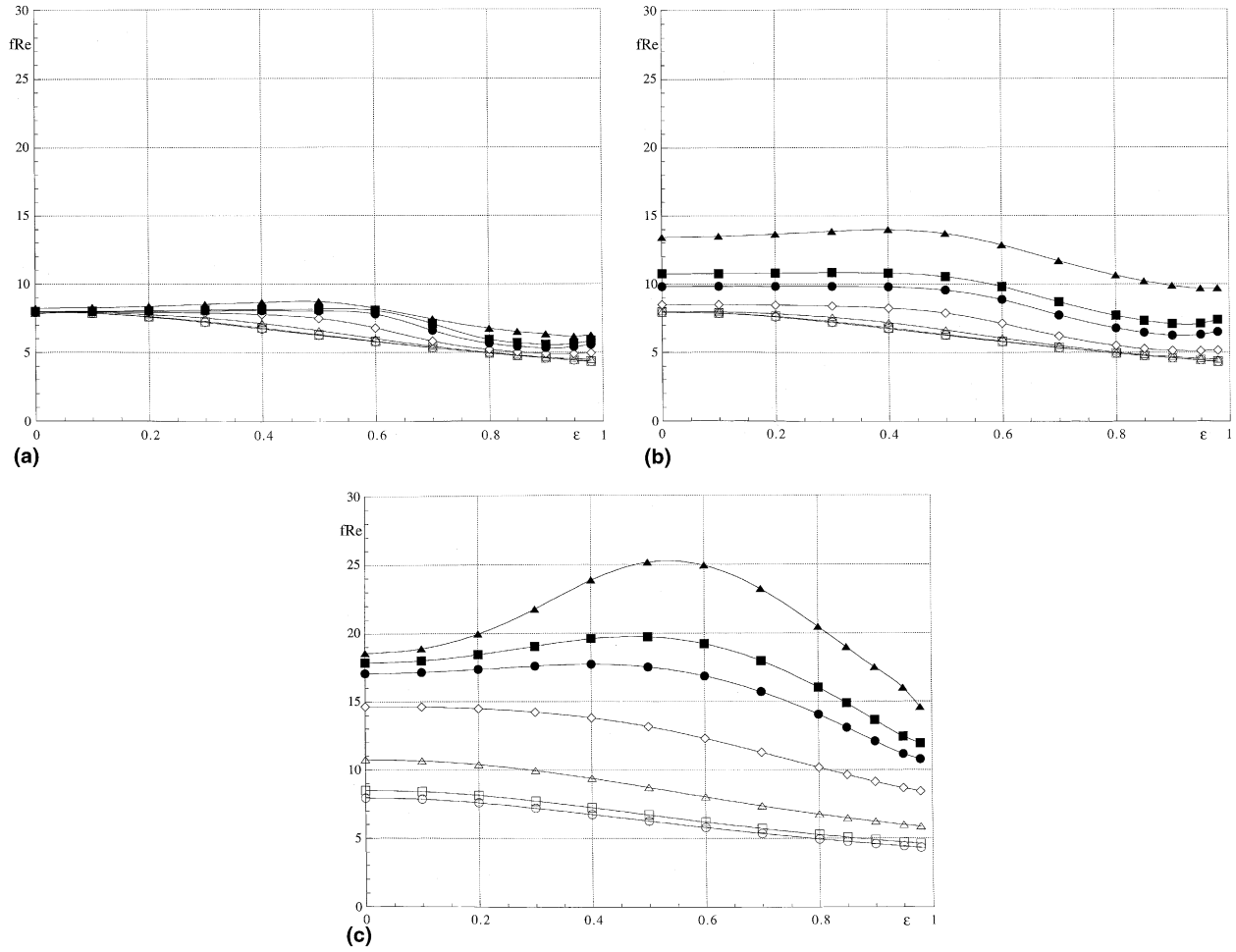

Fig. 5. Influence of Taylor number on $f \cdot Re$ versus Re for $\kappa = 0.5$, $n_{PL} = 0.5$ and (a) $Re = 1000$, (b) $Re = 100$, (c) $Re = 10$: (○) $Ta = 0$, (□) $Ta = 10$, (△) $Ta = 100$, (◇) $Ta = 10\,000$, (●) $Ta = 5000$, (■) $Ta = 10\,000$, (▲) $Ta = 50\,000$.

independent of Re for $\xi \to \infty$ i.e. the case of very high rotation speeds or very low Re, as is evident from the equations of Section 2. At high eccentricities and high Ta, $f \cdot Re$ actually exceeds that for Newtonian fluids because of the changes in the flowfield created by the effect of rotation on the viscosity field.

Finally, Fig. 6 shows the influence of the radius ratio κ. Shear thinning reduces $f \cdot Re$ for low and high radius ratios as it did for the intermediate value $\kappa = 0.5$ which was used in the previous figures. Perhaps surprisingly, at least for the case of $Ta = 10^4$ and $Re = 10^2$, the $f \cdot Re$ variation with κ becomes monotonic for all values of eccentricity in contrast with the more complex variation for Newtonian fluids.

4. Sensitivity to rheology

The sensitivity of calculated $f \cdot Re$ values to the viscometric model adopted has been assessed by comparing values resulting from the power-law model with results for the Carreau, Cross, and Herschel–Bulkley models, including simplified versions of Carreau and Cross with zero values of the infinite shear-rate viscosity μ_∞. This sensitivity analysis shows the extent to which the adoption of the simple power-law viscosity model is an adequate representation of fluids which are better fitted by more sophisticated viscosity models incorporating additional free parameters. The procedure for matching the parameters of the power-law fluid to those of the other viscosity models is outlined in Appendix A. The non-dimensional geometrical parameters adopted for the comparisons are $\kappa = 0.5$, $\varepsilon = 0$ and $\varepsilon = 0.7$. The numerical calculations are carried out using dimensional variables for which the reference values are $R_I = 25.4$ mm, $U = 0.12451$ m/s, $\omega = 0.98039$ rad/s, and $\rho = 10^3$ kg/m^3. These values correspond to a characteristic shear rate for the flow $\dot{\gamma}_F = 2.5$ s^{-1}. For a power-law fluid with $K_{PL} = 0.1$ Pa $\cdot$ s$^{n_{PL}}$ and $n_{PL} = 0.5$, both Re and Ta assume the value 100 whereas for other rheology models not only does the friction factor change but also the Reynolds and Taylor numbers. The results of the

Table 1
Results of power-law calculations: dependence of $f \cdot Re$ on n_{PL}, κ, ε, Ta and Re

ε	Ta						
	0	10	10^2	10^3	10^4	5×10^4	
(a) $n_{PL} = 0.8,\ \kappa = 0.5,\ Re = 10^2$							
0.0	15.438	15.443	15.489	15.874	17.451	18.890	
0.10	15.236	15.245	15.325	15.813	17.471	18.995	
0.20	14.663	14.683	14.842	15.606	17.507	19.273	
0.30	13.811	13.840	14.072	15.176	17.462	19.572	
0.40	12.794	12.825	13.078	14.413	17.131	19.515	
0.50	11.719	11.745	11.958	13.239	16.198	18.600	
0.60	10.659	10.675	10.815	11.760	14.513	16.852	
0.70	9.6656	9.6735	9.7461	10.308	12.577	15.001	
0.80	8.7619	8.7664	8.8100	9.1881	11.055	13.553	
0.85	8.3463	8.3517	8.4022	8.8102	10.625	13.055	
0.90	7.9549	7.9633	8.0376	8.5662	10.523	12.808	
0.95	7.5872	7.6008	7.7169	8.4532	10.782	12.977	
0.98	7.3776	7.3955	7.5453	8.4440	11.065	13.322	
	0	10	10^2	10^3	5×10^3	10^4	5×10^4
(b) $n_{PL} = 0.5,\ \kappa = 0.5,\ Re = 10^2$							
0.0	7.9468	7.9531	8.0094	8.4973	9.8219	10.751	13.437
0.10	7.8572	7.8726	7.9662	8.4905	9.8279	10.766	13.498
0.20	7.5955	7.6336	7.8291	8.4646	9.8406	10.802	13.663
0.30	7.2048	7.2624	7.5757	8.3994	9.8414	10.834	13.870
0.40	6.7428	6.8040	7.1792	8.2445	9.7836	10.798	13.965
0.50	6.2605	6.3101	6.6457	7.8793	9.5496	10.549	13.696
0.60	5.7895	5.8211	6.0510	7.1207	8.8597	9.8113	12.850
0.70	5.3510	5.3670	5.4960	6.2032	7.7354	8.6860	11.686
0.80	4.9518	4.9595	5.0276	5.5095	6.7902	7.7067	10.641
0.85	4.7675	4.7742	4.8342	5.2743	6.4521	7.3312	10.220
0.90	4.5932	4.6014	4.6722	5.1341	6.2533	7.0800	9.8687
0.95	4.4286	4.4416	4.5448	5.1127	6.3022	7.1148	9.6785
0.98	4.3342	4.3520	4.4864	5.1673	6.5099	7.3828	9.6959
	0	10	10^2	10^3	10^4	5×10^4	
(c) $n_{PL} = 0.2,\ \kappa = 0.5,\ Re = 10^2$							
0.0	3.8874	3.8921	3.9338	4.2988	6.2320	9.5576	
0.10	3.8699	3.8792	3.9288	4.2991	6.2323	9.5689	
0.20	3.7776	3.8216	3.9110	4.2977	6.2461	9.6019	
0.30	3.6160	3.7095	3.8750	4.2926	6.2597	9.6520	
0.40	3.4223	3.5366	3.8071	4.2801	6.2721	9.7043	
0.50	3.2261	3.3205	3.6699	4.2511	6.2731	9.7170	
0.60	3.0403	3.1013	3.3738	4.1749	6.2242	9.5879	
0.70	2.8740	2.9049	3.0553	3.8560	5.9405	9.1365	
0.80	2.7160	2.7336	2.8198	3.2385	5.2300	8.4145	
0.85	2.6446	2.6571	2.7252	3.0914	4.9526	8.0801	
0.90	2.5768	2.5865	2.6475	2.9833	4.7420	7.8048	
0.95	2.5123	2.5230	2.5933	2.9324	4.6019	7.5755	
0.98	2.4752	2.5064	2.5775	2.9649	4.6353	7.4563	
	0	10	10^2	10^3	10^4	5×10^4	
(d) $n_{PL} = 0.5,\ \kappa = 0.8,\ Re = 10^2$							
0.0	7.9994	8.0264	8.2550	9.7343	13.247	15.294	
0.10	7.8860	7.9248	8.1993	9.7166	13.273	15.469	
0.20	7.5704	7.6333	8.0190	9.6523	13.327	15.926	
0.30	7.1154	7.1938	7.6815	9.5021	13.332	16.427	
0.40	6.5915	6.6668	7.1711	9.1790	13.152	16.615	
0.50	6.0548	6.1131	6.5439	8.5441	12.591	16.163	
0.60	5.5399	5.5781	5.8491	7.5656	11.495	14.993	
0.70	5.0646	5.0865	5.2917	6.5262	10.042	13.439	
0.80	4.6345	4.6486	4.7924	5.7392	8.6649	11.871	
0.85	4.4366	4.4512	4.5938	5.4900	8.1261	11.122	
0.90	4.2497	4.2682	4.4295	5.3436	7.7828	10.417	
0.95	4.0733	4.0994	4.2968	5.2904	7.7240	10.049	
0.98	3.9723	4.0048	4.2309	5.2966	7.8444	10.326	

Table 1 (*continued*)

ε	*Ta*						
	0	10	10^2	10^3	10^4	5×10^4	
(e) $n_{PL} = 0.5,\ \kappa = 0.2,\ Re = 10^2$							
0.0	7.7196	7.7212	7.7345	7.8633	8.8298	10.931	
0.10	7.6770	7.6791	7.6958	7.8396	8.8249	10.937	
0.20	7.5346	7.5386	7.5693	7.7655	8.8087	10.952	
0.30	7.2975	7.3040	7.3573	7.6363	8.7751	10.964	
0.40	6.9879	6.9977	7.0724	7.4386	8.7062	10.948	
0.50	6.6397	6.6505	6.7328	7.1487	8.5556	10.835	
0.60	6.2816	6.2909	6.3626	6.7487	8.2091	10.468	
0.70	5.9349	5.9410	5.9883	6.2652	7.5587	9.7483	
0.80	5.6169	5.6653	5.6427	5.7400	6.9058	9.0967	
0.85	5.4707	5.5023	5.4945	5.5569	6.6612	8.7504	
0.90	5.3330	5.3662	5.3684	5.4378	6.4429	8.5006	
0.95	5.2064	5.2349	5.2500	5.3349	6.3290	8.4326	
0.98	5.1344	5.1675	5.1988	5.2820	6.3098	8.4130	
	0	10	10^2	10^3	5×10^3	10^4	5×10^4
(f) $n_{PL} = 0.5,\ \kappa = 0.5,\ Re = 10$							
0.0	7.9468	8.4973	10.751	14.660	17.078	17.850	18.553
0.10	7.8572	8.4065	10.662	14.621	17.156	18.005	18.891
0.20	7.5955	8.1404	10.394	14.491	17.361	18.444	19.950
0.30	7.2048	7.7320	9.9544	14.236	17.601	19.055	21.758
0.40	6.7428	7.2358	9.3750	13.807	17.720	19.592	23.849
0.50	6.2605	6.7094	8.7124	13.163	17.528	19.733	25.164
0.60	5.7895	6.1925	8.0238	12.296	16.869	19.221	24.937
0.70	5.3510	5.7115	7.3608	11.266	15.699	17.980	23.220
0.80	4.9518	5.2727	6.7567	10.175	14.060	16.024	20.475
0.85	4.7675	5.0759	6.4837	9.6384	13.097	14.880	18.982
0.90	4.5932	4.8880	6.2309	9.1234	12.089	13.635	17.513
0.95	4.4286	4.7113	5.9983	8.6640	11.162	12.441	16.000
0.98	4.3342	4.6105	5.8706	8.4348	10.770	11.939	14.591
	0	10	10^2	10^3	5×10^3	10^4	5×10^4
(g) $n_{PL} = 0.5,\ \kappa = 0.5,\ Re = 10^3$							
0.0	7.9468	7.9469	7.8573	7.9531	7.9784	8.0094	8.2417
0.10	7.8572	7.8664	7.9051	7.9490	7.9857	8.0209	8.2717
0.20	7.5955	7.6278	7.7712	7.9334	8.0062	8.0536	8.3670
0.30	7.2048	7.2571	7.5237	7.8909	8.0346	8.1026	8.5214
0.40	6.7428	6.7994	7.1345	7.7820	8.0573	8.1568	8.6649
0.50	6.2605	6.3061	6.6061	7.4993	8.0355	8.1877	8.7291
0.60	5.7895	5.8175	6.0082	6.7911	7.8048	8.0712	8.2287
0.70	5.3510	5.3635	5.4513	5.8328	6.6172	7.1070	7.4490
0.80	4.9518	4.9570	4.9956	5.2166	5.6626	5.9587	6.7673
0.85	4.7675	4.7721	4.8088	5.0290	5.4402	5.7107	6.5268
0.90	4.5932	4.5998	4.6505	4.9163	5.3327	5.5750	6.3421
0.95	4.4286	4.4400	4.5246	4.9018	5.2042	5.6456	6.1734
0.98	4.3342	4.3504	4.4671	4.9550	5.5823	5.8638	6.2557

comparisons are given in Table 2 presented in terms of the percentage difference Δ between the values of f_{PL} and f_{NN}, defined as

$$\Delta = 100\left(1 - \frac{f_{PL}}{f_{NN}}\right) \tag{26}$$

the subscript "PL" indicating the power-law result and "NN" the result for the particular model being assessed. The friction factor f_{NN} in each case is obtained from the definition $-\delta(\partial p/\partial z)/(\rho U^2)$, the axial pressure gradient $\partial p/\partial z$ being one of the key results of the numerical calculations.

So far as Table 2 is concerned, we can draw a number of conclusions. For the simplified Cross and Carreau models (i.e. $\mu_\infty = 0$), the difference Δ increases as the characteristic shear rate for the fluid ($\dot{\gamma}_{SCR,1}$ or $\dot{\gamma}_{SCA,1}$) increases and approaches that for the flow ($\dot{\gamma}_F$). The difference is higher for the simplified Cross model than for the simplified Carreau model because the change from power-law behaviour to the low-shear-rate Newtonian plateau is less gradual for the latter. In general, for a difference of less than 5%, we conclude that $\dot{\gamma}_{SCR}/\dot{\gamma}_F$ must be less than 0.01 whereas the corresponding value of $\dot{\gamma}_{SCA,1}/\dot{\gamma}_F$ is 0.4.

Table 2
Sensitivity of calculations to viscosity model

ε	μ_0 (Pa s)	μ_∞ (Pa s)	λ_{CR} (s)	m_{CR}	n_{PL}	K_{PL} (Pa $s^{n_{PL}}$)	$\dot{\gamma}_{CR,I}$ (s^{-1})	$\dot{\gamma}_{CR,1}$ (s^{-1})	$\dot{\gamma}_{CR,2}$ (s^{-1})	$10^2 f_{CR}$	$10^2 f_{PL}$	Δ (%)	Re
(a) *Cross model*													
0	10	10^{-3}	10^4	0.5	0.50990	0.10000	1.0	8.302×10^{-5}	12045	8.3908	8.1897	2.4	99.1
		10^{-2}			0.53070	0.10731	0.1	6.369×10^{-5}	157	11.884	8.5805	28	86.9
0.7	10	10^{-3}	10^4	0.5	0.50990	0.10000	1.0	8.302×10^{-5}	12045	5.7149	5.5994	2.0	99.1
		10^{-2}			0.53070	0.10731	0.1	6.369×10^{-5}	157	7.7722	5.8124	25	86.9

ε	μ_0 (Pa s)	μ_∞ (Pa s)	λ_{SCR} (s)	m_{SCR}	n_{PL}	K_{PL} (Pa $s^{n_{PL}}$)	$\dot{\gamma}_{SCR,1}$ (s^{-1})	$10^2 f_{SCR}$	$10^2 f_{PL}$	Δ (%)	Re
(b) *Simplified Cross model*											
0	10	0	10^4	0.5	0.5	0.1	10^{-4}	7.9925	8.0094	−0.21	101
	1		10^2				10^{-2}	7.8426		−2.1	106
	0.1		1				1	6.6077		−21	163
0.7	10	0	10^4	0.5	0.5	0.1	10^{-4}	5.4830	5.4960	−0.24	101
	1		10^2				10^{-2}	5.3687		−2.4	106
	0.1		1				1	4.4545		−2.3	163

ε	μ_0 (Pa s)	μ_∞ (Pa s)	m_{CA}	n_{PL}	K_{PL} (Pa $s^{n_{PL}}$)	$\dot{\gamma}_{CA,I}$ (s^{-1})	$\dot{\gamma}_{CA,1}$ (s^{-1})	$\dot{\gamma}_{CA,2}$ (s^{-1})	$10^2 f_{CA}$	$10^2 f_{PL}$	Δ (%)	Re
(c) *Carreau model*												
0	1	10^{-4}	0.5	0.50050	0.10009	0.6933	9.97×10^{-3}	1.016×10^6	8.0488	8.0185	0.38	99.9
		10^{-3}		0.50330	0.10080	0.2764	9.86×10^{-3}	1.080×10^4	8.4008	8.0691	3.9	98.5
		10^{-2}		0.52020	0.10677	0.1108	9.44×10^{-3}	1.392×10^2	11.829	8.3812	29	87.1
0.7	1	10^{-4}	0.5	0.50050	0.10009	0.6933	9.97×10^{-3}	1.016×10^6	5.5188	5.5010	0.32	99.9
		10^{-3}		0.50330	0.10080	0.2764	9.86×10^{-3}	1.080×10^4	5.7233	5.5289	3.4	98.5
		10^{-2}		0.52020	0.10677	0.1108	9.44×10^{-3}	1.392×10^2	7.7373	5.6988	26	87.1

ε	μ_0 (Pa s)	μ_∞ (Pa s)	λ_{SCA} (s)	n_{PL}	K_{PL} (Pa $s^{n_{PL}}$)	$\dot{\gamma}_{SCA}$ (s^{-1})	$10^2 f$	$10^2 f_{PL}$	Δ (%)	Re
(d) *Simplified Carreau model*										
0	1.0	0	100	0.5	0.1	10^{-2}	8.0095	8.0094	0	100
	0.316		10			10^{-1}	8.0095		0	100
	0.1		1			1	8.0003		−0.11	104
	0.032		0.1			10	7.5579		−6.0	203
0.7	1.0	0	100	0.5	0.1	10^{-2}	5.4960	5.4960	0	100
	0.316		10			10^{-1}	5.4960		0	100
	0.1		1			1	5.4868		−0.17	104
	0.032		0.1			10	5.0396		−9.1	203
ε	τ_Y (Pa)	n_{HB}	K_{HB} (Pa $s^{n_{HB}}$)	n_{PL}	K_{PL} (Pa $s^{n_{PL}}$)	$\dot{\gamma}_{HB}$ (s^{-1})	$10^2 f_{HB}$	$10^2 f_{PL}$	Δ (%)	Re
(e) *Herschel–Bulkley model*										
0	10^{-3}	0.5	0.1	0.5	0.1	10^{-4}	7.9423	8.0094	−0.85	99.4
	10^{-2}					10^{-2}	8.0958		1.1	94.1
	0.05					0.25	8.7736		8.7	76.0
	0.1					1	9.6109		17.	61.3
0.7	10^{-3}	0.5	0.1	0.5	0.1	10^{-4}	5.4445	5.4960	−0.95	99.4
	10^{-2}					10^{-2}	5.5622		1.2	94.1
	0.05					0.25	6.0824		9.6	76.0
	0.1					1	6.7273		18	61.3

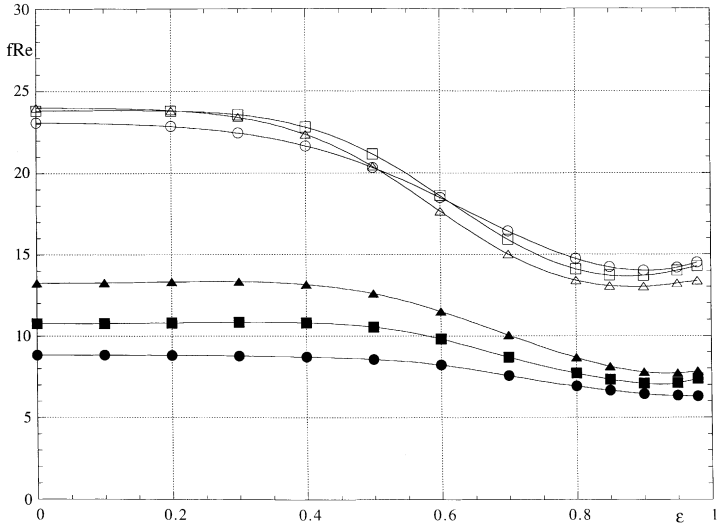

Fig. 6. Influence of radius-ratio κ on $f \cdot Re$ versus ε for $n_{PL} = 0.5$, $Re = 100$, $Ta = 10000$: (●) $\kappa = 0.2$, (■) $\kappa = 0.5$, (▲) $\kappa = 0.8$. Reference curves for $n_{PL} = 1$: (○) $\kappa = 0.2$, (□) $\kappa = 0.5$, (△) $\kappa = 0.8$.

For the full Cross and Carreau models, the trend is less straightforward but depends primarily on the second characteristic shear rate ($\dot{\gamma}_{CR,2}$ or $\dot{\gamma}_{CA,2}$) resulting from the power-law intersection with μ_∞. For the Cross model the difference is large if $\dot{\gamma}_F/\dot{\gamma}_{CR,2} > 0.016$ and falls to well below 2% if $\dot{\gamma}_F/\dot{\gamma}_{CR,2} < 2 \times 10^{-4}$. For the Carreau model the difference is again large if $\dot{\gamma}_F/\dot{\gamma}_{CA,2} > 0.016$ but less than 3% if the ratio is below 2.3×10^{-4} and less than 1% if it is less than 2.5×10^{-6}. For the Herschel–Bulkley model the situation is similar to that for the simplified Cross and Carreau models except that, because the deviation from the power law is very slow at low shear rates, the difference becomes large if the characteristic shear rate for the fluid, $\dot{\gamma}_{HB}$, is low. For $\dot{\gamma}_{HB}/\dot{\gamma}_F < 4 \times 10^{-3}$ the difference is less than 5%.

Although these conclusions are based upon calculations for a value of $\dot{\gamma}_F = 2.5\ s^{-1}$, it is anticipated that similar conclusions would hold for flows characterised by different values of $\dot{\gamma}_F$.

5. Comparison with results of Meuric et al. (1998) for a power-law fluid

Meuric et al. (1998) present results of numerical simulations for the flow of power-law fluids through eccentric annuli with inner-cylinder rotation. In agreement with the findings of Escudier et al. (2000), for a Newtonian fluid ($n_{PL} = 1$) they find increasing flow rate with eccentricity while increased levels of rotation reduce throughflow. For a shear-thinning fluid ($n_{PL} = 0.7$) the simulations of Meuric et al. (represented in their Figure 12 by the symbol △) show that for $\varepsilon = 0.3$ and 0.7 the flow rate initially decreases with rotation speed, then tends to level and finally increases. For $\varepsilon = 0.5$, on the other hand, the flowrate again levels out after the initial decrease but decreases again at the highest rotation speed. We believe this behaviour may be attributable to a lack of accuracy associated with the coarseness of their mesh. Their results also suggest that higher levels of eccentricity result in a steeper decrease of flow rate with rotation rate and a shift of the condition of minimum flow rate to higher rotation speeds. Meuric et al. fit straight lines through their calculated results indicating a decrease in flowrate with rotation speed which they also state to be the case in the text. This interpretation suggests that they doubted the accuracy of their numerical calculations to the point of not accepting some of the qualitative trends.

Unfortunately lack of information about the geometry and imposed pressure gradient in the paper of Meuric et al. did not allow us to attempt to reproduce their simulations. We have nevertheless attempted to determine whether the trends of their predictions are consistent with ours. Also, an important difference is that while Meuric et al. calculated the axial flow rate for a given pressure gradient, in our code the flow rate is an input parameter and the pressure gradient a result, and the trends observed in our figures must therefore be inverted in order to correspond to the variables used by Meuric et al.

In Fig. 7 the computed pressure gradient for a fluid with $n_{PL} = 0.5$, $K_{PL} = 0.1\ Pa \cdot s^{n_{PL}}$ is plotted against the rotation speed ω for several different eccentricities in the range 0–0.75 at two different values of the axial bulk velocity (0.1 and 0.2 m/s) and for a fluid with $n_{PL} = 0.8$, $K_{PL} = 0.1\ Pa \cdot s^{n_{PL}}$, $U = 0.1185$ m/s and eccentricities up to 0.7. For a concentric annulus the pressure gradient always decreases with rotation rate

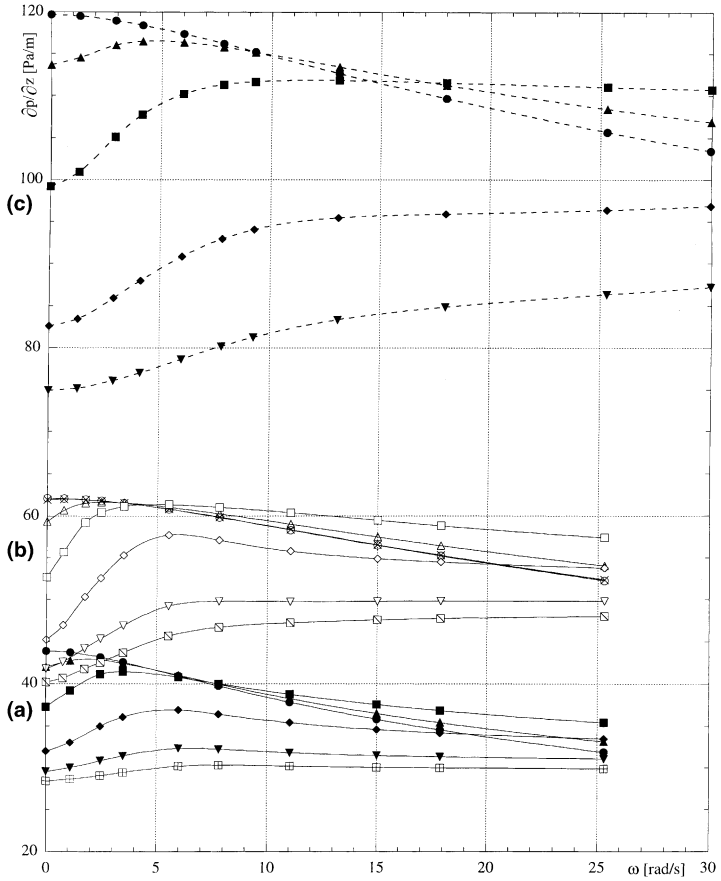

Fig. 7. Axial pressure gradient versus inner-cylinder rotation speed for $R_I = 25.4$ mm, $\kappa = 0.5$, $K = 0.1$ Pa $s^{n_{PL}}$: (a) $U = 0.1$ m/s, $n_{PL} = 0.5$, (●) $\varepsilon = 0$, (▲) $\varepsilon = 0.2$, (■) $\varepsilon = 0.4$, (◆) $\varepsilon = 0.6$, (▼) $\varepsilon = 0.7$, (⊞) $\varepsilon = 0.75$, (b) $U = 0.2$ m/s, $n_{PL} = 0.5$, (○) $\varepsilon = 0$, (×) $\varepsilon = 0.05$, (△) $\varepsilon = 0.2$, (□) $\varepsilon = 0.4$, (◇) $\varepsilon = 0.6$, (▽) $\varepsilon = 0.7$, (⧅) $\varepsilon = 0.75$, (c) $U = 0.12$ m/s, $n_{PL} = 0.8$, (●) $\varepsilon = 0$, (▲) $\varepsilon = 0.2$, (■) $\varepsilon = 0.4$, (◆) $\varepsilon = 0.6$, (▼) $\varepsilon = 0.7$.

and it is duct eccentricity that promotes the maximum pressure drop (or minimum flow rate in Meuric et al.). We note also that the rotation rate at which there is a maximum pressure gradient increases with eccentricity as well as with bulk velocity. For instance, with $U = 0.2$ m/s the pressure gradient maximum is hardly detectable for $\varepsilon = 0.7$ and entirely absent for $\varepsilon = 0.75$. That this phenomenon is enhanced by shear thinning can also be confirmed from the curves for a bulk velocity $U = 0.1185$ m/s. For $\varepsilon = 0.7$ the pressure gradient now exhibits no maximum, whereas in both previous cases there were maxima for this eccentricity. The highest rotation rates for the curves in Fig. 7 correspond to Taylor numbers well in excess of 50 000, a value that is unlikely to be attained in practice without the onset of instabilities.

The overall conclusion is that, for shear-thinning fluids in eccentric annuli, the flow rate decreases to a minimum as the rotation rate increases at a constant pressure gradient as shown by the detailed results of Meuric et al. The trend is accentuated for intermediate eccentricities but diminishes with increasing Reynolds number.

6. Conclusions

Friction factors and other kinematic characteristics have been obtained for the flow of power-law fluids through eccentric annuli with inner-cylinder rotation by carrying out a large number of computations (over 400 computer runs) covering a wide range of the relevant parameters: tabulated results are provided for $n_{PL} = 0.2$, 0.5, 0.8; $\kappa = 0.2$, 0.5, 0.8; $\varepsilon = 0$–0.98; $Re = 10$, 10^2, 10^3; $Ta = 0$, 10, 10^2, 10^3, 10^4, 5×10^4. The graphical results cover a selected range of these parameters to illustrate the major trends. This study has extended considerably existing knowledge of this type of flow represented by the works of Fang et al. (1999) (no rotation), Meuric et al. (1998), (restricted range of parameters given in terms of dimensional variables) and Wan et al. (2000) (restricted range of parameters). The work has also revealed that some of the conclusions of Meuric et al. are misleading and that some of the results of Beverly and Tanner (1992) are in error.

In general, the $f \cdot Re$ values for power-law fluids follow the trends observed by Escudier et al. (2000) for Newtonian fluids, including an increase with Ta, an increase with

eccentricity at low and very high ε but a decrease for intermediate ε. These effects result from the distortion of the axial velocity field created by the combined effects of eccentricity and inner-cylinder rotation. However, due to its shear thinning characteristics, a power-law fluid generally exhibits lower friction factors compared with the Newtonian fluid, or the power law at higher n_{PL}, a feature also documented in other studies (Meuric et al., 1998; Wan et al., 2000). Our study is sufficiently extensive to suggest a practical classification of the annular flow of shear-thinning fluids in terms of the velocity ratio $\xi \equiv \omega R_I/U$ which is directly related to the non-dimensional shear rate $\gamma_F = \sqrt{(1+\xi^2)}/2$. For $\xi < 1$ the flow is dominated by the axial throughflow and shear thinning creates a low viscosity layer around the inner cylinder which reduces $f \cdot Re$ at all eccentricities and the $f \cdot Re$ versus ε curve tends to that for $Ta = 0$. At the other extreme ($\xi > 10$) the flow is rotation dominated and $f \cdot Re$ becomes dependent in a complex way on whether there is a recirculation region in the cross-flow plane. For high values of Ta and ε, the effect of the inner-cylinder low-viscosity layer is counteracted by the appearance of a high viscosity region within the low-velocity ($\ll \omega \cdot R_I$) recirculation in the vicinity of the outer wall of the annulus as a consequence of which the shear stress on the outer cylinder wall is very high and hence $f \cdot Re$ increases. This effect is so strong that at low Reynolds numbers, $f \cdot Re$ may even exceed the value for the corresponding Newtonian flow, a very surprising characteristic not previously reported. Also, at very high rotation rates ($Ta = 5 \times 10^4$) and intense shear thinning ($n_{PL} = 0.2$), flow recirculation disappears completely in contrast to the situation for higher n_{PL} values including unity (i.e. the Newtonian case). In the intermediate range ($1 < \xi < 10$), the flow has a mixed behaviour and $f \cdot Re$ increases with ξ.

We propose and demonstrate that the results for power-law fluids can be applied to fluids characterised by other rheological models by an appropriate choice of the power-law index n_{PL} and the consistency index K_{PL} depending upon the ratios of the characteristic shear rate for the flow to the characteristic shear rates for the fluid. In Appendix A of the present paper we develop a systematic matching procedure to determine n_{PL} and K_{PL} which we apply to the Cross, Carreau and Herschel–Bulkley models. Confidence in the accuracy of any of the approximate approaches to the annular flow problem, which are more likely to be used in practice, can be achieved through comparison with our numerical solutions. It cannot be taken for granted that an inelastic viscosity model will be adequate in all circumstances except perhaps for the calculation of axisymmetric flows which are regarded as what Astarita and Marucci (1974) term viscometric. As Alves et al. (in press) have shown in a recent paper, for an axisymmetric flow the crucial issue is whether the viscosity function adopted for the inelastic model captures the exact shear viscosity behaviour of a viscoelastic fluid which is influenced by the elastic normal stresses. Also, it should not be forgotten that no account has been taken in the calculations for viscoelastic effects due to the elongational viscosity. The normal stress would be expected to affect any flow in an eccentric annulus (see e.g. Davies and Li, 1994) whereas the elongational viscosity only plays a role for the eccentric annulus with inner cylinder rotation. Extensive comparisons (Escudier et al., 2001) between the results of calculations and experimental data suggest that for the flows under consideration accurate results are obtained in spite of the neglect of viscoelastic effects.

Appended to the paper is an extensive bibliography of 100 (Appendix B) papers not specifically referred to in the text concerning theoretical and numerical investigations of laminar flow of non-Newtonian fluids through annular channels.

Acknowledgements

The financial support of EPSRC/MTD (research grant GR/F87813), Shell Research BV and British Gas plc is gratefully acknowledged by M.P. Escudier. P.J. Oliveira and F.T. Pinho acknowledge the receipt of sabbatical leave grants by FCT (grants FMRH/BSAB/68/98 and BLS 68/97). The authors' names are listed in alphabetical order.

Appendix A. Matching the power-law model to the Cross, Carreau and Herschel–Bulkley models and determination of characteristic shear rates

For the calculations reported in Section 4, to determine sensitivity to the viscosity model, it was necessary to select values for the parameters K_{PL} and n_{PL} so that the power-law model $\mu_{PL} = K_{PL}\dot{\gamma}^{n_{PL}-1}$ was appropriately matched to more sophisticated viscosity models. As we discuss below, the choice of a consistent matching procedure was influenced by the characteristics of the Cross model.

A.1. Cross model

The Cross model is almost invariably plotted in log–log coordinates and so appears to exhibit a lower Newtonian plateau for $\dot{\gamma} \to 0$, an upper Newtonian plateau for $\dot{\gamma} \to \infty$, and a sigmoidal curve with an inflexion point at intermediate shear rates. In fact, as is clear from the original paper by Cross (1965), the Cross-model equation

$$\mu_{CR} = \mu_\infty + \frac{\mu_0 - \mu_\infty}{1 + (\lambda_{CR}\dot{\gamma})^{m_{CR}}} \tag{A.1}$$

produces a curve with no inflexion point and no true asymptotic behaviour: $d\mu_{CR}/d\dot{\gamma}$ approaches infinity as $\dot{\gamma}$ approaches zero and μ_{CR} approaches the value μ_0. It is the logarithmic "stretching" at low shear rates which gives the impression of a first Newtonian plateau since $d(\ln\mu)/d(\ln\dot{\gamma})$ tends to zero as $\dot{\gamma}$ tends to zero. Thus the Cross model exhibits neither power-law behaviour at high shear rates nor an inflexion point in linear coordinates (i.e. μ_{CR} versus $\dot{\gamma}$). For the present work, therefore, to approximate the Cross model the power-law parameters were determined by matching the slope and viscosity at the inflexion point $\dot{\gamma}_{CR,I}$ in log–log coordinates. The result is

$$\dot{\gamma}_{CR,I} = \frac{1}{\lambda_{CR}}\left(\frac{\mu_0}{\mu_\infty}\right)^{1/2m_{CR}} \tag{A.2}$$

from which

$$n_{PL} = 1 - m_{CR}\frac{(\mu_0-\mu_\infty)(\mu_0/\mu_\infty)^{1/2}}{\mu_I\left[1+(\mu_0/\mu_\infty)^{1/2}\right]^2} \tag{A.3}$$

and

$$K_{PL} = \frac{\mu_I}{\dot{\gamma}_{CR,I}^{n_{PL}-1}}, \tag{A.4}$$

where

$$\mu_I = \mu_\infty + \frac{(\mu_0-\mu_\infty)}{1+(\mu_0/\mu_\infty)^{1/2}} \tag{A.5}$$

is the viscosity at the inflexion point, $\mu_I(\dot{\gamma}_{CR,I})$.

The first characteristic shear rate $\dot{\gamma}_{CR,1}$ is determined by the intersection point between $\mu=\mu_0$ and the power-law line which, for this model, is given by

$$K_{PL}\dot{\gamma}_{CR,1}^{n_{PL}-1} = \mu_0 \quad \text{or} \quad \dot{\gamma}_{CR,1} = \dot{\gamma}_{CR,I}\left(\frac{\mu_0}{\mu_I}\right)^{1/(n_{PL}-1)}. \tag{A.6}$$

The second characteristic shear rate $\dot{\gamma}_{CR,2}$ is determined from the intersection with μ_∞ so that

$$K_{PL}\dot{\gamma}_{CR,2}^{n_{PL}-1} = \mu_\infty$$

or

$$\dot{\gamma}_{CR,2} = \dot{\gamma}_{CR,I}\left(\frac{\mu_\infty}{\mu_I}\right)^{1/(n_{PL}-1)}. \tag{A.7}$$

This method of fitting a power-law equation to the Cross model is illustrated in Fig. 8, for two different sets of parameters.

A simplified version of the Cross model results from setting $\mu_\infty = 0$ so that

$$\mu_{SCR} = \frac{\mu_0}{1+\left(\lambda_{SCR}\dot{\gamma}\right)^{m_{SCR}}}. \tag{A.8}$$

This model then predicts power-law behaviour at high shear rates and a Newtonian region at low shear rates. The power-law parameters are given by

$$n_{PL} = 1 - m_{SCR} \quad \text{and} \quad K_{PL} = \mu_0\lambda_{SCR}^{-m_{SCR}} \tag{A.9}$$

and the characteristic shear rate $\dot{\gamma}_{SCR}$ by

$$\mu_0 = K_{PL}\dot{\gamma}_{SCR}^{n_{PL}-1} \quad \text{or} \quad \dot{\gamma}_{SCR} = 1/\lambda_{SCR}. \tag{A.10}$$

There is, of course, no second characteristic shear rate when $\mu_\infty = 0$.

A.2. Carreau model

In contrast to the Cross model, the Carreau model does exhibit a Newtonian plateau at low shear rates and

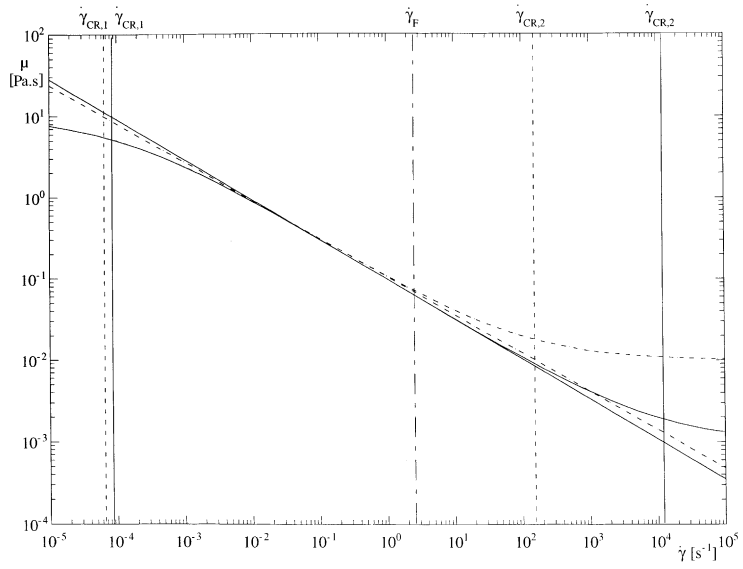

Fig. 8. Illustration of the method for matching the power-law model (straight lines) to the Cross model with $\lambda_{CR} = 10^4$ s, $\mu_0 = 10$ Pa s and (a) $\mu_\infty = 10^{-3}$ Pa s, $K_{PL} = 0.1$ Pa $s^{n_{PL}}$, $n_{PL} = 0.5099$ (——), (b) $\mu_\infty = 10^{-2}$ Pa s, $K_{PL} = 0.1073$ Pa $s^{n_{PL}}$, $n_{PL} = 0.5307$ (– – –).

an inflexion point in linear–linear coordinates. However, for consistency with the Cross-model matching procedure, it was decided to select the power-law parameters to match the Carreau model at the inflexion point $\dot{\gamma}_{CA,I}$ in log–log coordinates

$$\mu_{CA} = \mu_\infty + \frac{\mu_0 - \mu_\infty}{[1 + (\lambda_{CA}\dot{\gamma})^2]^{m_{CA}}}. \tag{A.11}$$

Unfortunately the determination of $\dot{\gamma}_{CA,I}$ now requires numerical solution of the transcendental equation

$$\left[1 - m_{CA}(\lambda_{CA}\dot{\gamma}_{CA,I})^2\right]\left[1 + (\lambda_{CA}\dot{\gamma}_{CA,I})^2\right]^{m_{CA}} + \frac{\mu_0}{\mu_\infty} - 1 = 0. \tag{A.12}$$

It can be shown that

$$n_{PL} = 1 - 2m_{CA}\frac{(\mu_0 - \mu_\infty)(\lambda_{CA}\dot{\gamma}_{CA,I})^2}{\mu_I[1 + (\lambda_{CA}\dot{\gamma}_{CA,I})^2]^{1+m_{CA}}} \tag{A.13}$$

and

$$K_{PL} = \frac{\mu_I}{\dot{\gamma}_{CA,I}^{n_{PL}-1}}, \tag{A.14}$$

where

$$\mu_I = \mu_\infty + \frac{\mu_0 - \mu_\infty}{[1 + (\lambda_{CA}\dot{\gamma}_{CA,I})^2]^{m_{CA}}} \tag{A.15}$$

and the first characteristic shear rate $\dot{\gamma}_{CA,1}$ for the Carreau model is given by

$$\mu_0 = K_{PL}\dot{\gamma}_{CA,1}^{n_{PL}-1}. \tag{A.16}$$

The second characteristic shear rate is given by

$$\mu_\infty = K_{PL}\dot{\gamma}_{CA,2}^{n_{PL}-1}. \tag{A.17}$$

As with the Cross model, a simplified version of the Carreau model results from setting $\mu_\infty = 0$ i.e.

$$\mu_{SCA} = \mu_0[1 + (\lambda_{SCA}\dot{\gamma})^2]^{(n_{SCA}-1)/2}, \tag{A.18}$$

and this also has a power-law asymptote at high shear rates. The power-law parameters are again selected to ensure a match with this asymptote i.e.

$$K_{PL} = \mu_0\lambda_{SCA}^{n_{SCA}-1} \quad \text{and} \quad n_{PL} = n_{SCA}. \tag{A.19}$$

A characteristic shear rate for this fluid $\dot{\gamma}_{SCA}$ is then given by

$$\mu_0 = K_{PL}\dot{\gamma}_{SCA}^{n_{PL}-1} \quad \text{or} \quad \dot{\gamma}_{SCA} = 1/\lambda_{SCA}. \tag{A.20}$$

A.3. Herschel–Bulkley model

Much the same reasoning as for the simplified Cross and Carreau models applies to the Herschel–Bulkley model which has no inflection point and also asymptotes to power-law behaviour at high shear rates. We have now

$$\tau_{HB} = \tau_Y + K_{HB}\dot{\gamma}^{n_{HB}} \tag{A.21}$$

or

$$\mu_{HB} = \frac{\tau_Y}{\dot{\gamma}} + K_{HB}\dot{\gamma}^{n_{HB}-1} \tag{A.22}$$

so that

$$K_{PL} = K_{HB} \quad \text{and} \quad n_{PL} = n_{HB}. \tag{A.23}$$

Since the viscosity for the Herschel–Bulkley model becomes infinite at zero shear rate, in this case a characteristic shear rate for the fluid is defined by matching the shear stress at zero shear rate i.e. τ_Y, to that given by the power law i.e.

$$\dot{\gamma}_{HB} = \left(\frac{\tau_Y}{K_{HB}}\right)^{1/n_{HB}}. \tag{A.24}$$

Here again, there is no second characteristic shear rate because μ_{HB} tends to zero as $\dot{\gamma}$ tends to infinity.

Appendix B. Bibliography of additional papers concerned with theoretical aspects of laminar flow of non-Newtonian liquids through annular ducts

Concentric annulus, no rotation

Anshus, B.E., 1974. Bingham plastic flow in annuli. Ind. Eng. Chem Fundam. 13 (2), 162–164.

Ashare, E., Bird, R.B., Lescarboura, J.A., 1965. Falling cylinder viscometer for non-Newtonian fluids. AIChE J. 11 (5), 910–916.

Batra, R.L., Jena, B., 1990. Entrance region flow of blood in concentric annulus. Int. J. Eng. Sci. 28, 407–419.

Batra, R.L., Sudarsan, V.R., 1992. Laminar flow and heat transfer in the entrance region of concentric annuli for power law fluids. Comput. Meth. Appl. Mech. Eng. 95, 1–16.

Bergman, P.D., 1962. Laminar flow of non-Newtonian fluids in annuli. M.Sc., Thesis, Purdue University.

Bhatnagar, R.K., 1963. Steady laminar flow of visco-elastic fluid through a pipe and through an annulus with suction or injection at the walls. J. Ind. Inst. Sci. 45, 126–151.

Bird, R.B., Dai, G.C., Yarusso, B.Y., 1983. The rheology and flow of viscoplastic materials. Rev. Chem. Eng. 1 (1), 1–70.

Bittleston, S.H., Fordham, E.J., 1994. Comments on Gücüyener and Mehmetoglu (1992). AIChE J. 40 (2), 378–379.

Buchtelova, M., 1988. Comments on "The axial laminar flow of yield pseudoplastic fluids in a concentric annulus". Ind. Eng. Chem. Res. 27, 1557–1558.

Capobianchi, M., Irvine, T.F., 1992. Predictions of pressure drop and heat transfer in concentric annular ducts with modified power law fluids. Wärme u Stoffübertr 27, 209–215.

Chen, S.S., Fan, L.T., Hwang, C.L., 1970. Entrance region flow of the Bingham fluid in a circular pipe. AIChE J. 16 (2), 293–299.

Chien, S.-F., 1970. Laminar flow pressure loss and flow pattern transition of Bingham plastics in pipes and annuli. Int. J. Mech. Miner. Sci. 7, 339–356.

David, J., Filip, P., 1994. Explicit solution of laminar tangential flow of power-law fluids in concentric annuli. Acta Technica CSAV 39, 539–544.

David, J., Filip, P., 1994. Quasisimilarity of flow behaviour of power-law fluids in concentric annuli. Fluid Dyn. Res. 14, 63–70.

David, J., Filip, P., 1996. Explicit pressure drop-flow rate relation for laminar axial flow of power-law fluids in concentric annuli. J. Pet. Sci. Eng. 16, 203–208.

David, J., Filip, P., 1995. Relationship of annular and parallel-plate Poiseuille flows for power-law fluids. Polym.-Plast. Technol. Eng. 34 (6), 947–960.
Grodde, K.-H., 1953. Beiträge zur Rheologie disperser Systeme. Erdöl und Kohle 6 (7), 380–384.
Gücüyener, H.I., Mehmetoglu, T., 1992. Flow of yield-pseudo-plastic fluids through a concentric annulus. AIChE J. 38 (7), 1139–1143.
Gupta, R.K., Chhabra, R.P., 1996. Laminar flow of power law fluids in concentric annuli. AIChE J. 42 (7), 2080–2083.
Hanks, R.W., Larsen, K.M., 1979. The flow of power-law non-Newtonian fluids in concentric annuli. Ind. Eng. Chem. Fundam. 18 (1), 33–35.
Hong, S.-N., Matthews, J.C., 1969. Heat transfer to non-Newtonian fluids in laminar flow through concentric annuli. Int. J. Heat Mass Transfer 12, 1699–1703.
Jaisinghani, R.A., 1974. Annular flow of a Casson fluid. MS Thesis, University of Wisconsin – Milwaukee, USA.
Jensen, T.B., Sharma, M.P., 1987. Study of friction factor and equivalent diameter correlations for annular flow of non-Newtonian drilling fluids. ASME J. Energy Resour. Technol. 109, 200–205.
Kanaka Raju, K., Devanathan, R., 1971. Heat transfer to non-Newtonian fluids in laminar flow through concentric annuli with or without suction. Rheol. Acta 10, 484–492.
Kozicki, W., Tiu, C., 1971. Improved parametric characterisation of flow geometries. Can. J. Chem. Eng. 49 (October), 562–569.
Lin, S.H., Hsu, C.C., 1980. Generalised Couette flow of a non-Newtonian fluid in annuli. Ind. Eng. Chem. Fundam. 19, 421–424.
Lin, S.H., Hsu, C.C., 1982. Response to comments on "Generalised Couette flow of a non-Newtonian fluid in annuli". Ind. Eng. Chem. Fundam. 21, 98–99.
Liu, J., Shah, V.L., 1975. Numerical solution of a Casson fluid flow in the entrance of annular tubes. Appl. Sci. Res. 31 (October), 213–222.
Machač, I., Doleček, P., Machačová, L., 1999. Poiseuille flow of purely viscous non-Newtonian fluids through ducts of non-circular cross section. Chem. Eng. Process 38, 143–148.
MacSporran, W., 1982. Comments on "Generalised Couette flow of a non-Newtonian fluid in annuli". Ind. Eng. Chem. Fundam. 21, 98.
Malik, S., Shenoy, U.V., 1991. Generalised annular Couette flow of a power-law fluid. Ind. Eng. Chem. Res. 30, 1950–1954.
Matsuhisa, S., Bird, R.B., 1965. Analytical and numerical solutions for laminar flow of the non-Newtonian Ellis fluid. AIChE J. 11 (4), 588–595.
McEachern, D.W., 1966. Axial laminar flow of a non-Newtonian fluid in an annulus. AIChE J. 12 (2), 328–332.
Melrose, J.C., Savins, J.G., Foster, W.R., Parish, E.R., 1958. A practical utilization of the theory of Bingham plastic flow in stationary pipes and annuli. Trans. Pet. AIME 213, 316–324.
Mishra, I.M., Kumar, S., Mishra, P., 1985. Entrance region flow of Bingham plastic fluids in concentric annulus. Ind. J. Tech. 23 (March), 81–87.
Mishra, I.M., Mishra, P., 1976. Flow behaviour of power law fluids in an annulus. AIChE J. 22 (3), 617–619.
Mishra, I.M., Mishra, P., 1977. Linearized approach for predicting loss coefficients in entrance region flows of purely viscous non-Newtonian fluids in an annular duct. Chem. Eng. J. 14, 41–47.
Mori, Y., Ototake, N., 1953. On the plastic flow through double concentric tube. Chem. Eng. (Japan) 1 (6), 224–229 (in Japanese, summary in English).
van Olphen, H., 1950. Pumpability, rheological properties and viscometry of drilling fluids. J. Inst. Pet. 36, 223–234.
Pinho, F.T., Oliveira, P.J., 2000. Axial annular flow of a non-linear viscoelastic fluid – an analytical solution. J. Non-Newtonian Fluid Mech. 93, 325–337.
Prasanth, N., Shenoy, U.V., 1992. Poiseuille flow of a power-law fluid between coaxial cylinders. J. Appl. Polym. Sci. 46, 1189–1194.
Remorino, M.R., Tonini, R.D., Böhm, U., 1979. Mass transfer to the inner wall of an annulus with non-Newtonian fluids. AIChE J. 25 (2), 368–370.
Round, G.F., Yu, S., 1993. Entrance laminar flows of viscoplastic fluids in concentric annuli. Can. J. Chem. Eng. 71, 642–645.
Savins, J.G., 1958. Generalised Newtonian (pseudoplastic) flow in stationary pipes and annuli. Trans. AIME 213, 325–332.
Shchipanov, P.K., 1949. Flow of viscoplastic material in the concentric space between two coaxial tubes. J. Tech. Phys. 19 (10), 1211–1214 (in Russian).
Shah, V.L., 1980. Blood flow. In: Mujundar, A.S., Mashelkar, R.A. (Eds.), Advances in Transport Processes, vol. 1, pp. 1–57.
Shul'man, Z.P., 1973. Calculation of a laminar axial flow of a nonlinear viscoplastic medium in an annular channel. J. Eng. Phys. 19, 1283–1289.
Slibar, A., Paslay, P.R., 1957. Die axiale Strömung von Bingham Plastiken in konzentrischen Rohren. ZAMM 37 (11/12), 441–449.
Tanaka, M., Mitsuishi, N., 1974. Non-Newtonian laminar heat transfer in concentric annuli. Kagaku-Kogaku 38, 664–671 (in Japanese).
Tanaka, M., Mitsuishi, N., 1975. Non-Newtonian laminar heat transfer in concentric annuli. Heat Transfer Jpn. Res. 4, 26–36.
Tiu, C., Bhattacharyya, S., 1973. Flow behaviour of power-law fluids in the entrance region of annuli. Can. J. Chem. Eng. 51 (February), 47–54.
Tuoc, T.K., McGiven, J.M., 1994. Laminar flow of non-Newtonian fluids in annuli. Trans. I Chem. E (A) 72 (September), 669–676.
Vaughn, R.D., 1963. Laminar flow of non-Newtonian fluids in concentric annuli. Soc. Pet. Eng. J. 3 (December), 274–276.
Volarovich, M.P., Gutkin, A.M., 1963. On the flow of viscoplastic disperse systems in the clearance between two coaxial tubes. Kolloid Z. 25 (6), 642–645 (in Russian).
Wadhwa, Y.D., 1966. Generalized Couette flow of an Ellis fluid. AIChE J. 12 (5), 890–893.
Wein, O., Nebrensky, J., Wichterle, K., 1970. Non-Newtonian flow in annuli. Rheol. Acta 9 (2), 278–282.
Worth, R.A., 1979. Accuracy of the parallel-plate analogy for representation of viscous flow between coaxial cylinders. J. Appl. Polym. Sci. 24, 319–328.

Concentric annulus, inner-cylinder rotation

Bhattacharya, S.N., Javadpour, 1992. Helical flow of Herschel Bulkley fluids. In: Moldenaers, P., Keunings, R. (Eds.), Theoretical and Applied Rheology, Proceedings of the XI International Congress on Rheology, Brussels, Belgium, pp. 896–898.
Bittleston, S.H., Hassager, O., 1992. Flow of viscoplastic fluids in a rotating concentric annulus. J. Non-Newtonian Fluid Mech. 42, 19–36.
Coleman, B.D., Noll, W., 1959. Helical flow of general fluid. J. Appl. Phys. 30 (10), 1508–1512.
Dierckes, A.C., Schowalter, W.R., 1966. Helical flow of a non-Newtonian polyisobutelene solution. Ind. Eng. Chem. Fundam. 5 (2), 263–271.
Dostál, M., Zitný, R., Šesták, J., Houška, M., 1993. Helical flow of power-law fluids. AIChE J. 39 (1), 189–192.
Fredrickson, A.G., 1960. Helical flow of an annular mass of visco-elastic fluid. Chem. Eng. Sci. 11, 252–259.
Haiqiao, Z., Haiqing, C., 1985. The helical flow of the power law fluid in an annular space. In: Proceedings of the International Conference on Nonlinear Mechanics, October 28–31, Shanghai, China, pp. 834–839.
Kaloni, P.N., 1965. On the helical flow of an elasto-viscous fluid. Ind. J. Pure Appl. Phys. 3, 1–3.

Kulshrestha, P.K., 1962. Helical flow of an idealized elastico-viscous liquid (I). ZAMP XIII, 553–561.
Luo, Y., Peden, J.M., 1990. Laminar annular helical flow of power-law fluids. Part 1: Various profiles and axial flow rates. SPE 20304.
Naimi, M., Devienne, R., Lebouche, M., 1990. Etude dynamique et thermique de l'écoulement de Couette–Taylor–Poiseuille; cas d'un fluide présentant un seuil d'écoulement. Int. J. Heat Mass Transfer 33 (2), 381–391.
Paslay, P.R., Slibar, A., 1957. Laminar flow of drilling mud due to axial pressure gradient and external torque. Pet. Trans. AIME 210, 310–317.
Paslay, P.R., Slibar, A., 1958. Criterion for flow of a Bingham plastic between two cylinders loaded by torque and pressure gradient. ASME J. Appl. Mech. (June), 284–285.
Rao, D.K.M., 1965. Helical flow of a Bingham plastic. J. Ind. Inst. Sci. 47, 97–105.
Savins, J.G., Wallick, G.C., 1966. Viscosity profiles, discharge rates, pressures, and torques for a rheologically complex fluid in a helical flow. AIChE J. 12 (2), 357–363.
Tiu, C., Bhattacharyya, S., 1974. Developing and fully developed velocity profiles for inelastic power-law fluids in an annulus. AIChE J. 20 (6), 1140–1144.
Walker, R.E., Al-Rawi, O., 1970. Helical flow of bentonite slurries. J. Pet. Technol., September 1058 (abstract).
Wronski, S., Jastrzebski, M., 1980. Mass transfer from the wall to a helical flow of a power-law fluid. Pr. Inst. Inz. Chem. Politech. Warszawski IX (3), 239–248.
Wronski, S., Jastrzebski, M., 1990. Mass transfer in the spiral flow of a pseudoplastic liquid. Int. J. Heat Mass Transfer 33 (1), 1–7.
Wronski, S., Jastrzebski, M., Rudniak, L., 1988. Hydrodynamics of laminar helical flow of non-Newtonian liquids. Inz. Chem. Procesowa 9 (4), 713–721 (in Polish).

Eccentric annulus, no rotation

Azouz, I., Shirazi, S.A., Pilehvari, A., Azar, J.J., 1993. Numerical simulation of laminar flow of yield-power-law fluids in conduits of arbitrary cross-section. Trans. ASME J. Fluids Eng. 115, 710–716.
Fang, P., Manglik, R.M., 1996. Numerical solutions for laminar flows of viscous power-law fluids with heat transfer in eccentric annular channels. In: Abstract ASME National Heat Transfer Conference, Houston, USA, August.
Fang, P., Manglik, R.M., 1998. Numerical investigation of laminar forced convection in Newtonian and non-Newtonian flows in eccentric annuli. Technical Report No TFTPL-3, Department of Mechanical, Industrial and Nuclear Engineering, University of Cincinatti.
Haciislamoglu, M., 1989. Non-Newtonian fluid flow in eccentric annuli and its applications to petroleum engineering problems. Ph.D. Dissertation, Louisiana State University, USA.
Haciislamoglu, M., Langlinais, J., 1990. Non-Newtonian fluid flow in eccentric annuli. In: 1990 ASME Energy Resources Conference and Exhibition, New Orleans, pp, 115–123.
Haciislamoglu, M., Langlinais, J., 1990. Discussion of flow of a power law fluid in an eccentric annulus. SPE Drilling Eng. (March), 95.
Huilgol, R.R., Panizza, M.P., 1995. On the determination of the plug flow region in Bingham fluids through the application of variational inequalities. J. Non-Newtonian Fluid Mech. 58, 207–217.
Hussein, Q.E., Sharif, M.A.R., 1997. Viscoplastic fluid flow in irregular eccentric annuli. J. Energy Res. Tech. 120, 201–207.
Iyoho, A.W., Azar, J.A., 1981. An accurate slot-flow model for non-Newtonian fluid flow through eccentric annuli. Soc. Pet. Eng. J. (October), 565–572.
Luo, Y., Peden, J.M., 1987. Flow of drilling fluids through eccentric annuli. SPE 16692.
Patel, N., Ingham, D.B., 1992. The mixed convection flow of non-Newtonian fluids in parallel plate ducts and in eccentric annuli. ASME-HTD 201, 71–78.
Szabo, P., Hassager, O., 1992. Flow of viscoplastic fluids in eccentric annular geometries. J. Non-Newtonian Fluid Mech. 45, 149–169.
Tosun, I., Solmaz, S., Ozgen, C., 1995. Loss coefficients in entrance region flows of Newtonian and non-Newtonian fluids in eccentric annuli. Chem. Eng. Commun. 131, 207–224.
Tosun, I., Uner, D., Ozgen, C., 1987. Flow of the power law fluid in an eccentric annulus. SPE Paper 17002, 1–19.
Uner, D., Ozgen, C., Tosun, I., 1988. An approximate solution for non-Newtonian flow in eccentric annuli. Ind. Eng. Chem. Res. 27, 698–701.
Uner, D., Ozgen, C., Tosun, I., 1989. Flow of a power-law fluid in an eccentric annulus. SPE Drilling Eng. (September), 269–272.
Walton, I.C., Bittleston, S.H., 1991. The axial flow of a Bingham plastic in a narrow eccentric annulus. J. Fluid. Mech. 222, 39–60.
Wang, Y., 1998. Axial flow of generalized viscoplastic fluids in non-circular ducts. Chem. Eng. Commun. 168, 13–43.
Wang, Y., 1998. Noncircular duct flow of nonlinear viscoplastic fluids. J. Chin. Inst. Chem. Eng. 29 (2), 85–97.

Eccentric annulus, inner-cylinder rotation

Cui, H.-Q., Liu, X.-S., 1995. Research on helical flow of non-Newtonian fluids in eccentric annuli, SPE 29940. In: Proceedings of the International Meeting on Petroleum Engineering, Beijing, China, pp. 543–551.
Meuric, O.F.J., Chiu, T.W., Wakeman, R.J., Fisher, K.A., 1997. A numerical study of helical flow of generalised Newtonian fluids in eccentric annuli. Strojnicky Casopis 48 (5), 363–373.
Mori, N., Eguchi, T., Nakamura, K., Horikawa, A., 1985. Pressure flow of the non-Newtonian fluid in an eccentric double walled tube with a rotating inner cylinder. Part 1: Numerical calculation. J. Text. Mach. Soc. Jpn. 38 (2), 37–45 (in Japanese).
Zang, H.-Q., Wu, J.-Z., 1994. Analytical solutions of the helical flow of non-Newtonian fluid in eccentric annular space. App. Math. Mech. (English edition) 15, 657–670, Shanghai, China.

References

Alves, M.A., Pinho, F.T., Oliveira, P.J., in press. Study of steady pipe and channel flows of a single-mode Phan–Thien–Tanner fluid. J. Non-Newtonian Fluid Mech.
Astarita, G., Marucci, G., 1974. Principles of Non-Newtonian Fluid Mechanics. McGraw-Hill, New york.
Batra, R.L., Eissa, M., 1994. Helical flow of a Sutterby model fluid. Polym.-Plast. Technol. Eng. 33 (4), 489–501.
Beverly, C.R., Tanner, R.I., 1992. Numerical analysis of three-dimensional Bingham plastic flow. J. Non-Newtonian Fluid Mech. 42, 85–115.
Bird, R.B., 1965. Experimental tests of generalized Newtonian models containing a zero-shear viscosity and a characteristic time. Can. J. Chem. Eng. 75 (August), 161–168.
Chin, W.C., 2001. Computational Rheology for Pipeline and Annular Flow. Gulf Professional Publishing, Boston.
Cross, M.M., 1965. Rheology of non-Newtonian fluids: a new flow equation for pseudoplastic systems. J. Colloid Sci. 20, 417–437.
Davies, A.R., Li, X.K., 1994. Numerical modelling of pressure and temperature effects in viscoelastic flow between eccentrically rotating cylinders. J. Non-Newtonian Fluid Mech. 54, 331–350.
van Doormal, J.P., Raithby, G.D., 1984. Enhancements of the SIMPLE method for predicting incompressible fluid flows. Numer. Heat Transfer 7, 147–163.

Escudier, M.P., Gouldson, I.W., Oliveira, P.J., Pinho, F.T., 2000. Effects of inner cylinder rotation on laminar flow of a Newtonian fluid through an eccentric annulus. Int. J. Heat Fluid Flow 21, 92–103.

Escudier, M.P., Oliveira, P.J., Pinho, F.T., Smith, S., 2001. Fully developed laminar flow of non-Newtonian liquids through annuli: comparison of numerical calculations with experiments (submitted).

Fang, P., Manglik, R.M., Jog, M.A., 1999. Characteristics of laminar viscous shear-thinning fluid flows in eccentric annular channels. J. Non-Newtonian Fluid Mech. 84 (1), 1–18.

Ferziger, J.H., 1981. Numerical Methods for Engineering Application. Wiley, New York.

Fordham, E.J., Bittleston, S.H., Tehrani, M.A., 1991. Viscoplastic flow in centred annuli, pipes and slots. Ind. Eng. Chem. Res. 30 (3), 517–524.

Fredrickson, A.G., Bird, R.B., 1958. Non-Newtonian flow in annuli. Ind. Eng. Chem. 50 (3), 347–352.

Guckes, T.L., 1975. Laminar flow of non-Newtonian fluids in an eccentric annulus. J. Eng. Ind. (May), 498–506.

Haciislamoglu, M., Langlinais, J., 1990. Non-Newtonian fluid flow in eccentric annuli. J. Energy Res. Technol. 112, 163–169.

Hanks, R.W., 1979. The axial laminar flow of yield-pseudoplastic fluids in a concentric annulus. Ind. Eng. Chem. Process Des. Dev. 18 (3), 488–493.

Hussain, Q.E., Sharif, M.A.R., 1998. Helical flow of a pseudoplastic fluid in eccentric annuli. In: Proceedings of the ASME FEDSM'98, Washington, USA, June, pp. 1–6.

Hussain, Q.E., Sharif, M.A.R., 2000. Numerical modelling of helical flow of viscoelastic fluids in eccentric annuli. AIChE J. 46 (10), 1937–1946.

Issa, R.I., Oliveira, P.J., 1994. Numerical predictions of phase separation in two-phase flow through T-junctions. Comp. Fluids 23 (2), 347–372.

Kozicki, W., Chou, C.H., Tiu, C., 1966. Non-Newtonian flow in ducts of arbitrary cross-sectional shape. Chem. Eng. Sci. 21, 665–679.

Laird, W.M., 1957. Slurry and suspension transport. Basic flow studies on Bingham plastic fluids. Ind. Eng. Chem. 49 (1), 138–141.

Locket, T.J., 1992. Numerical simulation of inelastic non-Newtonian fluid flows in annuli. Ph.D. Thesis, University of London.

Meuric, O.F.J., Wakeman, R.J., Chiu, T.W., Fisher, K.A., 1998. Numerical flow simulation of viscoplastic fluids in annuli. Can. J. Chem. Eng. 76 (February), 27–40.

Mitsuishi, N., Aoyagi, Y., 1973. Non-Newtonian fluid flow in an eccentric annulus. J. Chem. Eng. Japan 6, 402–408.

Nebrenský, J., Ulbrecht, J., 1968. Non-Newtonian flow in annular ducts. Collect. Czech. Chem. Commun. 33, 363–375.

Nebrenský, J., Wein, O., Ulbrecht, J., 1970. Non-Newtonian flow in channels of annular cross section II, Ree–Eyring Fluid. Collect. Czech. Chem. Commun. 35, 1964–1971.

O'Donovan, E.J., Tanner, R.I., 1984. Numerical study of the Bingham squeeze film problem. J. Non-Newtonian Fluid Mech. 15, 75–83.

Oliveira, P.J., 1992. Computer modelling of multidimensional multiphase flow and application to T-junctions. Ph.D. Thesis, Imperial College of Science, Technology and Medicine.

Patankar, S.V., 1980. Numerical and Heat Transfer Fluid Flow. Hemisphere, Washington, DC.

Patankar, S.V., Spalding, D.B., 1972. A calculation procedure for heat, mass and momentum transfer in three-dimensional parabolic flows. Int. J. Heat Mass Transfer 15, 1787–1806.

Pearson, J.R.A., 1988. Rheological principles and measurements applied to the problems of drilling and completing oil wells. In: Proceedings of the Xth International Congress on Rheology, Sydney, vol. 1, pp. 73–78.

Pham, T.V., Mitsoulis, E., 1998. Viscoplastic flow in ducts. Can. J. Chem. Eng. 76, 120–125.

Rigbi, Z., Galili, N., 1971. Helical flow of some non-Newtonian liquids. Israeli J. Tech. 9 (5), 447–452.

Rivlin, R.S., 1956. Solution of some problems in the exact theory of visco-elasticity. J. Rat. Mech. Anal. 5 (1), 179–188.

Roache, P.J., 1997. Quantification of uncertainty in computational fluid mechanics. Ann. Rev. Fluid Mech. 29, 123–160.

Rotem, Z., 1962. Non-Newtonian flow in annuli. Trans. ASME J. Appl. Mech. (June), 421–424.

Russell, C.P., Christiansen, E.B., 1974. Axial, laminar, non-Newtonian flow in annuli. Ind. Eng. Chem. Process Des. Dev. 13 (4), 391–396.

Shul'man, Z.P., 1970. Calculation of a laminar axial flow of a nonlinear viscoplastic medium in an annular channel. Inzherno-Fizicheskii Zhurnal 19 (4), 689–697 (in Russian).

Vaughn, R.D., 1965. Axial laminar flow of non-Newtonian fluids in narrow eccentric annuli. Soc. Pet. Eng. J. (December), 277–280.

Volarovich, M.P., Gutkin, A.M., 1946. Flow of plastic-viscoplastic material between two parallel flat-walls and in annular space between two coaxial tubes. J. Tech. Phys. XVI (3), 321–328 (in Russian).

Wan, S., Morrison, D., Bryden, I.G., 2000. The flow of Newtonian and Inelastic non-Newtonian fluids in eccentric annuli with inner-cylinder rotation. Theor. Comp. Fluid Dyn. 13, 349–359.